

## Magnetostriction and Magnetoelastic Quantum Oscillations in $p$ -PbTe<sup>†</sup>

T. E. Thompson\*

*Department of Physics and Laboratory for Research on the Structure of Matter,  
University of Pennsylvania, Philadelphia, Pennsylvania 19104*

and

Paul R. Aron

*National Aeronautics and Space Administration,  
Lewis Research Center, Cleveland, Ohio 44135*

and

B. S. Chandrasekhar

*Department of Physics, Case Western Reserve University, Cleveland, Ohio 44106*

and

D. N. Langenberg

*Department of Physics and Laboratory for Research on the Structure of Matter,  
University of Pennsylvania, Philadelphia, Pennsylvania 19104*

(Received 8 March 1971)

A detailed experimental and theoretical study of quantum oscillations in the magnetostriction and Young's modulus of  $p$ -PbTe is presented. The valence band of PbTe is approximated by a spheroidal nonparabolic model in which the effects of strain on the valence-band parameters are described by a deformation potential model. Using appropriate thermodynamic derivatives of the modified Lifshitz-Kosevich expression for the oscillatory part of the electronic free energy, it is shown that both types of oscillations arise mainly from relative shifts of the valence-band maxima due to shear strains, accompanied by intervalley charge transfer. Band parameters derived from the periods, phases, and spin splitting of the oscillations are in generally good agreement with values reported by other workers. A detailed comparison is made of the experimentally observed oscillation amplitudes with those predicted by theory, and satisfactory agreement is found. The ratio of the amplitudes of the two effects yields a value of the valence-band deformation potential  $\Xi_v^v = 7.9 \pm 1.3$  eV in good agreement with a value found from piezoresistance experiments by Burke.

### I. INTRODUCTION

The Landau quantization of the energy levels of the conduction electrons in a solid placed in a magnetic field forms the basis for some of the most powerful techniques for establishing the electronic structure of solids.<sup>1</sup> One can construct, using the thermodynamic potential for the electronic system as calculated by Lifshitz and Kosevich, a free energy which is a function of the magnetic field, the temperature, and the elastic strain. The first derivatives of the free energy with respect to these three thermodynamic variables lead, respectively, to the magnetization, the entropy, and the elastic stress. Owing to the quantization of the electronic states, the free energy is periodic in the reciprocal of the magnetic field. This oscillatory character is consequently manifest in the magnetization, entropy, and stress.

The oscillatory magnetization (de Haas-van Alphen effect) has been most extensively used in the study of Fermi surfaces in metals. More recently, the oscillatory entropy, which is revealed as temperature oscillations in a thermally isolated crystal subjected to a swept magnetic field, has also been developed as a useful tool for such studies. The third effect, which appears as an os-

illatory magnetostriction, i. e., the dimensional change of a crystal placed in a magnetic field, forms one of the subjects of this paper. The elastic constants of the crystal, which are the second derivatives of the free energy with respect to strain, also show quantum oscillations, and form the second main topic of this paper.

We have measured the oscillatory behavior of the magnetostriction and the Young's modulus of single crystals of  $p$ -type lead telluride, a multi-valley degenerate semiconductor, and determined from these results the periods, phases, effective masses, and  $g$  factors for this material. From the amplitudes of these two quantities we have also determined the deformation potential  $\Xi_v^v$  for the valence band in lead telluride. The amplitude analysis is considerably simplified by using the ratio of the amplitudes of the two effects. This method of obtaining deformation potentials in semiconductors, or the generalized deformation parameters for Fermi surfaces in metals, is a new and important feature of the techniques described in this paper.

Magnetostriction (MS) was first observed by Joule, in 1842, in a bar of iron.<sup>2</sup> The main body of work since that time has been on ferromagnetic materials in which the effect is largest: The strains

in Fe and Ni are typically  $10^{-5}$ – $10^{-6}$  at the saturation field. The first observation of MS in a non-ferromagnetic material was made by Kapitza in 1929 in a series of classic experiments in pulsed fields up to 250 kG.<sup>3</sup> Kapitza observed a monotonic MS in Bi, Sb, graphite, Ga, Sn, and W, finding the effect to be greatest in Bi, where the strain  $\epsilon$  is  $\sim 10^{-5}$  in a field of 150 kG at room temperature.

In 1963, Chandrasekhar pointed out that oscillatory MS should be observable in materials which show the de Haas–van Alphen effect.<sup>4</sup> Subsequently, Green and Chandrasekhar observed the first such oscillations in Bi.<sup>5</sup> MS oscillations have since been observed in Ag,<sup>6</sup> As,<sup>7</sup> Be,<sup>8</sup> Bi,<sup>9</sup> Cd,<sup>10</sup> Cr,<sup>11</sup> Cu,<sup>6,12</sup> Ga,<sup>13</sup> GaSb,<sup>14</sup> PbTe,<sup>15,16</sup> Sb,<sup>17</sup> Sn,<sup>12,18</sup> and Zn.<sup>19</sup> One of us (Ref. 20) has observed MS oscillations in Au. The oscillatory strain amplitudes for these materials at 25 kG and temperatures near  $T = 4$  K range between  $10^{-6}$  and  $10^{-9}$ . For PbTe at this temperature and field,  $\epsilon \sim 10^{-7}$ .

Magnetostriction in diamagnetic systems is related directly to the strain dependence of the Fermi surface. Shoenberg<sup>21</sup> was one of the first to point out that the diamagnetic oscillatory magnetostriction could be analyzed in terms of the oscillatory magnetization  $M$  and the strain dependence of the appropriate extremal cross-sectional area of the Fermi surface:

$$\epsilon_i = -MB s_{ij}^0 \frac{\partial \ln S_m}{\partial \epsilon_j}, \quad (1.1)$$

where  $B$  is the magnetic field,  $s_{ij}^0$  is a component of the elastic compliance tensor, and  $S_m$  is the extremal cross-sectional area of the Fermi surface perpendicular to the applied magnetic field. (Throughout this paper we use the standard “engineering” form of the reduced stress and strain tensors.<sup>22</sup>) Equation (1.1) was derived using thermodynamic considerations together with the assumption that the strain dependence of the oscillatory diamagnetic free energy is dominated by the strain dependence of the  $S_m$  which appears in the argument of the oscillatory factor in the free energy.<sup>23</sup> The GaSb and Be experiments were analyzed using Eq. (1.1); a value for  $\partial \ln S_m / \partial \epsilon_j$  was found by measuring separately the magnetization and magnetostriction oscillations. In the present paper we derive an expression for the magnetostriction in terms of  $\partial \ln S_m / \partial \epsilon_j$ , directly from the total free energy, using a modified form of the Lifshitz-Kosevich expression for the diamagnetic free energy. We then use a simple multivalley deformation potential model to relate  $\partial \ln S_m / \partial \epsilon_j$  to the strain dependence of the PbTe valence band. A similar method has been used by Aron and Chandrasekhar for Bi<sup>9</sup> and by Belson *et al.* for PbTe.<sup>16</sup> However, the results and conclusions of Belson *et al.* differ from ours at several points.

An important new aspect of our analysis is the direct comparison of the MS oscillations with quantum oscillations in the elastic constants. By taking the ratio of the amplitudes of these two effects, the analysis is considerably simplified in a manner similar to the simplification obtained by taking the ratio of the amplitudes of the MS oscillations and the magnetization oscillations in Eq. (1.1).

Quantum oscillations in the velocity of sound were first reported by Mavroides *et al.* in Bi in 1962.<sup>24</sup> Velocity oscillations have since been reported in Al,<sup>25</sup> Au,<sup>26</sup> Be,<sup>27</sup> Ga,<sup>28</sup> and PbTe.<sup>29</sup> The amplitudes of these oscillations at 50 kG range from  $\Delta v/v \sim 10^{-5}$  for Au with  $T = 4$  K to  $\Delta v/v \sim 10^{-3}$  for Ga at 1.2 K. Sound-velocity oscillations due to geometric resonances in Al have also been observed with  $\Delta v/v \sim 10^{-5}$  at 2 kG for  $T = 4.2$  K.<sup>30</sup> The velocity oscillations in Ga and Bi have a spiked, or saw-tooth, appearance characteristic of giant quantum oscillations,<sup>31,32</sup> a special quantum effect which occurs when  $ql \gg 1$ , where  $q$  is the sound wave vector and  $l$  is the electron mean free path. The experiments in Au, Be, Al, and PbTe were carried out at frequencies such that  $ql \ll 1$ , and the oscillations have the sinusoidal appearance of de Haas–van Alphen oscillations.

In our experiments we have used a composite mechanical oscillator technique which measures the fractional change in Young’s modulus. To emphasize the fact that we measure oscillatory elastic-constant variations instead of sound-velocity variations, we call this effect *magnetoelastic (ME) oscillations*.

Theoretical treatments of the oscillatory magnetic field dependence of the velocity of sound have been given by Quinn and Rodriguez,<sup>33</sup> Rodriguez,<sup>34</sup> Blank and Kaner,<sup>35</sup> and Pustovoi and Poluéktoy<sup>36</sup> for electronic systems which have a simple spherical Fermi surface. Blank and Kaner investigated giant quantum oscillations. The others limited themselves to the case  $ql \ll 1$ , with Pustovoi and Poluéktoy emphasizing the effect of space charge associated with the ultrasonic wave. In their work on Ga, Neuringer and Shapira used the theory of Blank and Kaner to relate the amplitude of the giant quantum oscillations in the attenuation to the amplitude of the velocity oscillations.<sup>28</sup> They obtained better than order-of-magnitude self-consistency for the two effects. Rodriguez’s theory, which is meant to apply only to the case  $ql \ll 1$ , gives amplitudes which are four orders of magnitude smaller than the giant-quantum-oscillation amplitudes observed in Ga; however, Rodriguez’s theory gives order-of-magnitude agreement with the amplitudes observed in Al and Au.

Rodriguez derived an expression for the velocity oscillations by considering the electronic contribution to the bulk modulus. He simply calculated the

second derivative with respect to volume of the Lifshitz-Kosevich expression for the diamagnetic free energy of a free-electron gas, assuming the major contribution to this derivative to come from the strain dependence of the  $S_m$  which appears in the oscillatory factor, and using the free-electron expression  $\partial \ln S_m / \partial V = -\frac{2}{3}$ . This approach is quite similar to those mentioned above for calculating expressions for the MS oscillations. For the analysis of their Be experiments, Testardi and Condon derived expressions relating elastic-constant oscillations ( $ql \ll 1$ ) to magnetization oscillations.<sup>27</sup> They measured separately the magnetization and velocity oscillations and from the combined data report values of  $\partial \ln S_m / \partial \epsilon_j$ . The ideas behind their arguments are quite similar to those used to derive Eq. (1.1), where the magnetization and ME oscillations are related. Whereas Rodriguez's equations are limited to the free-electron gas, a ratio method such as that used by Testardi and Condon can be applied to an electronic system with a more general Fermi surface. Testardi and Condon also included  $B$ - $H$  effects and the interaction between strain and  $B$  in their analysis.

In Sec. II, we describe a spheroidal nonparabolic multivalley deformation potential model of the valence band of PbTe. In Sec. III, we derive theoretical expressions in terms of our valence-band model for the MS and ME oscillations from the appropriate strain derivatives of a modified form of the Lifshitz-Kosevich free energy. In Sec. IV we describe our experimental methods. In Sec. V A, band parameters obtained from our experimental results are compared with results previously obtained by other workers. Section V B presents an analysis of the amplitudes of the MS and ME oscillations and their ratio, leading to an experimental value of the valence-band deformation potential  $\Xi_v^v$  for PbTe. Section VI summarizes our conclusions. Some basic relationships for the spheroidal nonparabolic energy-band model are presented in the Appendix.

## II. PbTe VALENCE BAND

Lead telluride is a cubic (NaCl structure, point group  $m\bar{3}m$ ) degenerate semiconductor characterized (at liquid-helium temperatures) by a small energy gap ( $\sim 0.2$  eV), high carrier mobilities ( $\geq 10^5$  cm<sup>2</sup>V<sup>-1</sup>sec<sup>-1</sup>), and small effective masses ( $\sim 0.05m_0$ ). A mass of experimental evidence (de Haas-van Alphen oscillations, Shubnikov-de Haas oscillations, Azbel-Kaner cyclotron resonance, interband magneto-optical absorption, and other optical and transport phenomena<sup>37</sup>) indicates that the Fermi surface of both  $p$ - and  $n$ -type PbTe is well described by  $\langle 111 \rangle$ -directed prolate spheroids centered on the  $L$  points of the Brillouin zone

(Fig. 1). There are eight half-spheroids or, equivalently, four full spheroids in the zone.

Cuff, Ellett, and Kuglin<sup>38, 39</sup> found a strong carrier-concentration dependence of the  $\langle 111 \rangle$  cyclotron mass for  $p$ -type PbTe which indicates that the valence band of this material is nonparabolic. Dixon and Riedl<sup>40</sup> found similar results for the carrier-concentration dependence of the electric-susceptibility hole mass of PbTe. In order to take nonparabolicity into account, we use a model due largely to Kane<sup>41</sup> and Cohen.<sup>42</sup> Considering the symmetry of PbTe and using a coordinate system where  $p_3$  is the momentum component along  $[111]$ , and  $p_1$  and  $p_2$  are the components of the two orthogonal momenta, Cohen's Eq. (26) becomes

$$\frac{p_1^2 + p_2^2}{2m_1} = \left( E - \frac{p_3^2}{2m_3} \right) \left( 1 + \frac{E}{E_g} + \frac{p_3^2}{2E_g m_3'} \right), \quad (2.1)$$

where  $E_g$  is an effective energy gap between the valence and conduction bands,  $m_1$  and  $m_3$  are the band-edge effective masses, and  $m_3'$  is the longitudinal effective mass of the conduction band, which is experimentally found to be of the same order of magnitude as  $m_3$ .<sup>43</sup> The Fermi surface ( $E = E_F$ ) is more easily visualized by writing Eq. (2.1) in the form

$$E = (p_1^2 + p_2^2)/2m_1 + p_3^2/2m_3, \quad (2.2)$$

where

$$m_t = m_1 [1 + E/E_g + p_3^2/(2E_g m_3')], \quad (2.3)$$

$$m_l = m_3. \quad (2.4)$$

Equation (2.2) describes a surface of revolution about the 3 axis which has extremal cross sections at  $p_3 = 0$  and  $p_3^2 = m_3' E_g [(E/E_g)(m_3/m_3' - 1) - 1]$ . For the energy and mass values of our samples the position of the second extremum is imaginary, i. e., it does not exist, and Eq. (2.2) describes a

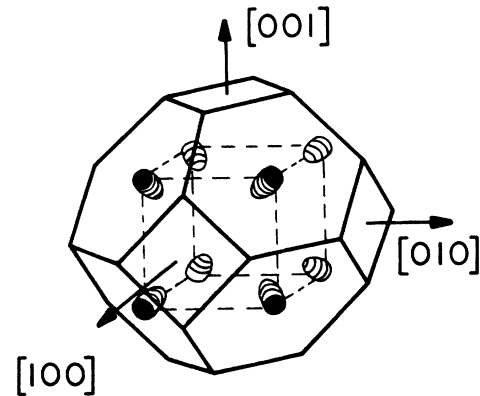


FIG. 1. Brillouin zone of PbTe showing the eight  $\langle 111 \rangle$ -directed half-spheroids which contain the carriers (either electrons or holes).

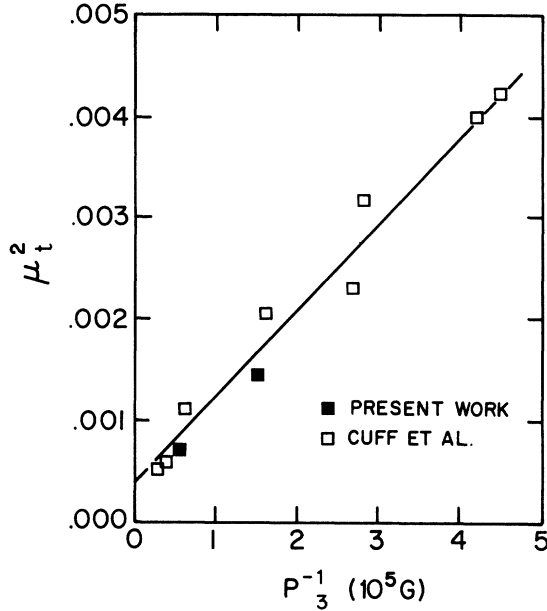


FIG. 2. Square of the normalized cyclotron mass versus the reciprocal period for  $B \parallel [111]$ . The intercept and slope are used to calculate  $m_1$  and  $E_g$  from Eq. (2.9).

Fermi surface which is spheroidal except for a slight bulging for large values of  $p_3$ . In this connection, we note that recent work by Schilz<sup>44</sup> indicates that when the carrier concentration becomes large ( $p > 5 \times 10^{18} \text{ cm}^{-3}$ ), the valence-band Fermi surface becomes cylinderlike in shape. The extremal cross section perpendicular to the  $p_3$  axis, located at  $p_3 = 0$ , is given by

$$S_{m_3} = 2\pi m_1 E (1 + E/E_g) . \quad (2.5)$$

The cyclotron orbits of importance in the present work do not traverse large values of  $p_3$ , so that the  $p_3$  dependence of the transverse mass indicated in Eq. (2.3) is small and can be neglected. Instead of Eq. (2.3) we therefore use

$$m_t = m_1 (1 + E/E_g) . \quad (2.6)$$

Equations (2.2), (2.4), and (2.6) describe the spheroidal nonparabolic model for the energy surfaces of *p*-type PbTe which we use throughout the remainder of this paper. As is conventional, we also define a mass anisotropy parameter  $K = m_1/m_t$ , which in our model has an energy dependence of the form  $K = (m_3/m_1)(1 + E/E_g)^{-1}$ .

A test of the validity of the model and an evaluation of the numerical values of the model parameters appropriate to *p*-PbTe can be made using our data and the data of Cuff *et al.* When the magnetic field is parallel to the unique axis of the spheroid, the quantum oscillation period  $P_3$  ( $E = E_F$ ) is

given by

$$P_3 \equiv \frac{e\hbar}{cS_{m_3}} = \frac{e\hbar}{cE_F m_1 (1 + E_F/E_g)} , \quad (2.7)$$

and the corresponding normalized cyclotron mass  $\mu_t$  is

$$\mu_t \equiv \frac{1}{2\pi m_0} \left. \frac{\partial S_{m_3}}{\partial E} \right|_{E=E_F} = \frac{m_1}{m_0} \left( 1 + 2 \frac{E_F}{E_g} \right) . \quad (2.8)$$

(For derivations of these relations, see the Appendix. In this paper  $\mu$  is always used to denote cyclotron masses normalized to  $m_0$ , the free-electron mass, and  $m$  is always used to denote unnormalized band masses. Notice that  $\mu_t m_0 \neq m_t$ .) Solving for  $E_F$  from Eq. (2.7), substituting this value of  $E_F$  into Eq. (2.8), and squaring the result gives the relation

$$\mu_t^2 = (m_1/m_0)^2 + C m_1 (P_3 E_g m_0)^{-1} , \quad (2.9)$$

where  $C = 4e\hbar/m_0c = 4.63 \times 10^{-8} \text{ eV G}^{-1}$ . Thus a plot of  $\mu_t^2$  versus  $P_3^{-1}$  gives the band-edge mass  $m_1$  and the energy gap  $E_g$ . Such an analysis was carried out by Cuff *et al.*,<sup>39</sup> and in Fig. 2 we show a plot of their data along with values found from this experiment. A least-squares fit of the data gives  $m_1 = (0.018 \pm 0.003) m_0$  and  $E_g = 0.10 \pm 0.02 \text{ eV}$ . A similar study of our data and that of Cuff *et al.* indicates that  $m_1$  is essentially constant over the range of carrier concentrations  $3.6 \times 10^{17} \text{ cm}^{-3} < p < 3.5 \times 10^{18} \text{ cm}^{-3}$  and has a value  $m_1 = m_3 = (0.19 \pm 0.02) m_0$ .

The direct gap  $\Delta$  between the valence and conduction bands of PbTe at  $T = 4.2 \text{ K}$  has been determined in two different experiments. Mitchell *et al.*<sup>45</sup> find  $\Delta = 0.190 \pm 0.002 \text{ eV}$  from magneto-optical studies of epitaxial films, and Butler and Calawa<sup>46</sup> find  $\Delta = 0.187 \text{ eV}$  from magnetoemission studies with PbTe diode lasers. The fact that the effective gap  $E_g$  in our model is smaller than the measured direct optical gap  $\Delta$  indicates that interactions between the valence band and the higher conduction-band states are important in determining the valence-band parameters.

The interaction of the electron spin with the magnetic field splits each Landau level by an amount  $\pm g e \hbar B / 4 m_0 c$ , where the electron  $g$  factor depends on the electron spin-orbit interaction. The two series of quantum oscillations associated with the two spin orientations interfere, producing a single set of quantum oscillations with an amplitude controlled by the factor  $\cos \frac{1}{2} \pi g \mu$ , where  $\mu$  is the normalized cyclotron mass appropriate to the applied field direction. Knowledge of this factor is important in our amplitude analysis.

The  $g$  factor is related to the components of a second-rank tensor and in PbTe has a directional dependence of the form

$$g^2 = g_{\parallel}^2 \cos^2 \theta + g_{\perp}^2 \sin^2 \theta, \quad (2.10)$$

where  $g_{\parallel}$  and  $g_{\perp}$  are the  $g$  factors for the field parallel and perpendicular to the [111] axis. The results of a number of different experiments (Table I) indicate that at the band edge,  $g_{\parallel} \approx 50$  and that  $g_{\perp}$  decreases with increasing carrier concentration. Burke *et al.*<sup>47</sup> find  $g_{\perp} = 7 \pm 2$ . The carrier-concentration dependence of  $g_{\parallel}$  is related to the nonparabolicity of the bands; the interband interactions which determine the  $g$  factor are quite similar to those which determine the inverse effective mass. To a first approximation, both experimentally and theoretically,<sup>48, 49</sup>  $g_{\parallel}$  varies with carrier concentration as  $1/m_t$ . Schilz<sup>44</sup> found the spin factor  $\frac{1}{2}g\mu$  to be directionally independent. This is borne out by other work: For example, using the values of Burke *et al.* and Eqs. (A9) and (2.10), we compute  $\frac{1}{2}g\mu = 0.56$  for the ellipsoid with the smallest extremal area when  $\vec{B}$  is along [110]. This value is sensibly the same as the values 0.58 shown in Table I for the [100] and [111] directions. Since we were able to measure the spin splitting only with  $\vec{B} \parallel [100]$ , we will assume the amplitude factor  $\cos \frac{1}{2}\pi g\mu$  to be the same for the [100], [110], and [111] directions.

The effect of strain on nondegenerate<sup>50</sup> energy levels in semiconductors can be described by a deformation potential tensor  $\overline{\Xi}$ .<sup>51-53</sup> In this scheme the shift in the energy of the point  $\nu$  in a band is described to first order in the strain  $\overline{\epsilon}$  by  $\delta E^{\nu} = \overline{\Xi}^{\nu} : \overline{\epsilon}$ . In general, each point in the band will have nine deformation potentials associated with it. However, this number is usually greatly reduced

at a symmetry point. At the  $L$  points in PbTe there are only two independent deformation potentials for each band, and we can express  $\overline{\Xi}^{\nu}$ , using the notation of Herring,<sup>52, 53</sup> as  $\overline{\Xi}_{ij}^{\nu} = \overline{\Xi}_d^{\nu} \delta_{ij} + \overline{\Xi}_u^{\nu} u_i^{\nu} u_j^{\nu}$ , where  $\delta_{ij}$  is the Kronecker  $\delta$  and the unit vector  $\hat{u}$  points to a particular  $L$  point. This leads to an energy shift of the form

$$\delta E^{\nu} = (\overline{\Xi}_d + \frac{1}{3}\overline{\Xi}_u)(\epsilon_1 + \epsilon_2 + \epsilon_3) + \frac{1}{3}\overline{\Xi}_u(\pm \epsilon_4 \pm \epsilon_5 \pm \epsilon_6), \quad (2.11)$$

where the signs depend upon  $\nu$ . The PbTe deformation potentials have been calculated by Ferreira.<sup>54</sup> However, there has been only a limited amount of experimental work on determining the PbTe deformation potentials. Ferreira's results are shown in Table II along with the deformation potentials derived from piezoresistance measurements by Ilisavskii<sup>55</sup> and Burke.<sup>56</sup> In order to find the deformation potential from piezoresistance, the elastic constants and the ratio of the mobilities perpendicular and parallel to the [111] axis must be known. Ilisavskii did not have good values for these two parameters, so we have corrected his deformation potentials using Burke's values. The variation of the energy gap with pressure has been measured optically<sup>57</sup> giving  $(3\overline{\Xi}_d^c + \overline{\Xi}_u^c) - (3\overline{\Xi}_d^v + \overline{\Xi}_u^v) = 9.5$  to 11.4 eV, where the superscripts refer to the valence or conduction bands. Ferreira's theoretical values give 11.6 eV, in reasonable agreement with experiment.

The band-edge masses  $m_1$  and  $m_3$  are found in the work of Lin and Kleinman<sup>37</sup> to be approximately given by  $m_0/m_i = M_i/\Delta$ , where the  $M_i$  ( $i = 1, 3$ ) are appropriate momentum matrix elements. Since we

TABLE I. Spin-splitting factors and  $g$  values for  $p$ -type PbTe. Subscripts  $\langle 100 \rangle$  indicate a  $\langle 100 \rangle$  magnetic field direction.

Experiment	Carrier conc ( $10^{18} \text{ cm}^{-3}$ )	$(\frac{1}{2}g\mu)_{\langle 100 \rangle}$	$\mu_{\langle 100 \rangle}$	$g_{\langle 100 \rangle}$	$\frac{1}{2}g_{\parallel} \mu_t$	$\mu_t$	$g_{\parallel}$
Butler and Calawa (Ref. 46)	0 <sup>a</sup>			29 <sup>b</sup>			
Cuff <i>et al.</i> (Ref. 39)	0						51 $\pm$ 8
Present work Sample X6	0.9	0.65 $\pm$ 0.05	0.041 $\pm$ 0.004 <sup>c</sup>	32 $\pm$ 4		0.027 $\pm$ 0.002	48 $\pm$ 5 <sup>d</sup>
Burke <i>et al.</i> (Ref. 47)	3.0	0.58 $\pm$ 0.01	0.051 $\pm$ 0.008	23 $\pm$ 5	0.58 $\pm$ 0.01	0.036 $\pm$ 0.002	32 $\pm$ 2
Present work Sample X5	3.5	0.55 $\pm$ 0.05	0.055 $\pm$ 0.002 <sup>c</sup>	20 $\pm$ 2		0.038 $\pm$ 0.001	29 $\pm$ 3 <sup>d</sup>
Schilz (Ref. 44)	4				0.58 $\pm$ 0.03 <sup>e</sup>	0.040 $\pm$ 0.008	29 $\pm$ 6
Schilz (Ref. 44)	6				0.53 $\pm$ 0.02 <sup>e</sup>	0.044 $\pm$ 0.009	24 $\pm$ 5

<sup>a</sup> $p$ - $n$  junction.

<sup>b</sup>Assuming conduction- and valence-band  $g$  factors equal.

<sup>c</sup>Computed from Eq. (A9).

<sup>d</sup>Assuming  $g\mu$  the same along  $\langle 111 \rangle$  and  $\langle 100 \rangle$ .

<sup>e</sup>Using a different splitting scheme than Schilz.

TABLE II. Deformation potentials of PbTe (eV).

Source	Valence band		Conduction band	
	$\Xi_d^v$	$\Xi_u^v$	$\Xi_d^c$	$\Xi_u^c$
Theory				
Ferreira (Ref. 54)	-8.93	10.46	-4.36	8.29
Experiment				
Ilisavskii (Ref. 55)	...	5.6 <sup>a</sup>	...	3.8 <sup>a</sup>
Burke (Ref. 56)	...	8.5	...	...

<sup>a</sup>Corrected values. (See text.)

expect these matrix elements to be insensitive to small strains, we find, using Eq. (2.11),

$$\frac{\partial \ln m_{1,3}}{\partial \epsilon_i} = \frac{\partial \ln \Delta}{\partial \epsilon_i} = \begin{cases} G_1/\Delta & \text{for } i=1, 2, \text{ or } 3 \\ \pm G_2/\Delta & \text{for } i=4, 5, \text{ or } 6, \end{cases} \quad (2.12)$$

where

$$G_1 = (\Xi_d^c - \Xi_d^v) + \frac{1}{3}(\Xi_u^c - \Xi_u^v), \quad G_2 = \frac{1}{3}(\Xi_u^c - \Xi_u^v), \quad (2.13)$$

and the sign depends upon the particular *L* point considered. Since the *g* values depend on the energy gap in a similar manner, they should have a similar type of strain dependence.

### III. THEORY

#### A. Thermodynamic Relations

We obtain theoretical expressions for the magnetostriction and magnetoelastic oscillations by considering the free-energy density of the crystal in a magnetic field as the sum of the zero-field elastic energy and the free energy of the diamagnetic electronic system,

$$F(\vec{\epsilon}, T, H) = \frac{1}{2} \sum_{i,j=1}^6 c_{ij}^0 \epsilon_i \epsilon_j + \Omega(\vec{\epsilon}, T, B) + 2\pi M^2, \quad (3.1)$$

where the  $c_{ij}^0$  are zero-field components of the elastic stiffness tensor. The magnetization can be obtained from this free energy as<sup>58</sup>  $M = -\partial F/\partial H = -\partial \Omega/\partial B$  and the stress as  $\sigma_i = \partial F/\partial \epsilon_i$ . Since we are interested in oscillatory effects, we need consider only the oscillatory part of  $\Omega$ . For this we use the Lifshitz-Kosevich expression in the modified form given by Williamson *et al.*<sup>59</sup>:

$$\Omega = \sum_{\nu} \sum_{\lambda=1}^{\infty} A_{\lambda\nu} \cos\left(\frac{\lambda c S_{\nu}^m}{e\hbar B} - \phi_{\lambda}\right). \quad (3.2)$$

$A_{\lambda\nu}$  is a temperature-dependent amplitude function which varies slowly with field,

$$A_{\lambda\nu} = 2kT \left(\frac{eB}{\hbar c}\right)^{3/2} \left| \frac{\partial^2 S^{\nu}}{\partial p_B^2} \right|_{S^{\nu}=S_{\nu}^m}^{-1/2} \frac{e^{-\lambda\alpha\mu_{\nu} T_D/B} \cos\frac{1}{2}\lambda\pi g_{\nu}\mu_{\nu}}{\lambda^{3/2} \sinh(\lambda\alpha\mu_{\nu} T/B)}, \quad (3.3)$$

where  $\mu_{\nu}$ ,  $g_{\nu}$ , and  $S_{\nu}^m$  are, respectively, the reduced cyclotron mass, effective *g* factor, and extremal cross-sectional area of the  $\nu$ th sheet of the Fermi surface,  $T_D$  is the Dingle temperature representing the effect of electron scattering, and  $\alpha = 2\pi^2 k m_0 c / \hbar e$ . The phase factor is  $\phi_{\nu} = 2\pi\lambda\gamma \pm \frac{1}{4}\pi$ , where  $\gamma$  is the phase associated with the Landau quantization and the upper sign is used when  $S_{\nu}^m$  is a maximum, the lower for a minimum. From Eq. (3.1) we find the general expression for the strain:

$$\epsilon_1 = \sum_{j=1}^6 s_{ij}^0 \left( \sigma_j - \frac{\partial \Omega}{\partial \epsilon_j} - 4\pi M \frac{\partial M}{\partial \epsilon_j} \right), \quad (3.4)$$

where the  $s_{ij}^0$  are defined by

$$\sum_{j=1}^6 s_{ij}^0 c_{jk}^0 = \delta_{ik}.$$

In PbTe, the magnetization is small enough so that the last term in Eq. (3.4) can be neglected. (Also, because of the smallness of *M*, the difference between *B* and *H* is inconsequential in our analysis.) The oscillatory magnetostriction in the [*l, m, n*] direction for a PbTe crystal with zero (or constant) external stresses is thus described by the equation

$$\epsilon_{lmn} = - \sum_{i,j=1}^6 \frac{\partial \epsilon_{lmn}}{\partial \epsilon_i} s_{ij}^0 \frac{\partial \Omega}{\partial \epsilon_j}, \quad (3.5)$$

where  $\partial \epsilon_{lmn}/\partial \epsilon_i$  is a product of direction cosines,  $\epsilon_{lmn} = l^2 \epsilon_1 + m^2 \epsilon_2 + n^2 \epsilon_3 + mn \epsilon_4 + ln \epsilon_5 + lm \epsilon_6$ .

The inverse of Young's modulus in the [*l, m, n*] direction is defined by  $(Y_{lmn})^{-1} \equiv \partial \epsilon_{lmn} / \partial \sigma_{lmn}$ ; therefore, the ME oscillations are given by

$$Y_{lmn}^{-1}(B) - Y_{lmn}^{-1}(0) \equiv \Delta(Y_{lmn})^{-1} = - \sum_{i,j,k,t=1}^6 \frac{\partial \epsilon_{lmn}}{\partial \epsilon_i} s_{ij}^0 \frac{\partial \sigma_k}{\partial \sigma_{lmn}} \frac{\partial \epsilon_t}{\partial \epsilon_j} \frac{\partial^2 \Omega}{\partial \epsilon_k \partial \epsilon_t}. \quad (3.6)$$

Using the identity  $\partial \sigma_k / \partial \sigma_{lmn} = \partial \epsilon_{lmn} / \partial \epsilon_k$  and the approximation  $\partial \epsilon_t / \partial \sigma_k \cong s_{tk}^0$ , the ME oscillations are thus described to first order in the elastic constants by

$$\Delta(Y_{lmn})^{-1} = - \sum_{i,j,k,t=1}^6 \frac{\partial \epsilon_{lmn}}{\partial \epsilon_i} \frac{\partial \epsilon_{lmn}}{\partial \epsilon_j} s_{ik}^0 s_{jt}^0 \frac{\partial^2 \Omega}{\partial \epsilon_k \partial \epsilon_t}. \quad (3.7)$$

#### B. Strain Derivatives of $\Omega$

In order to evaluate the strain derivatives of  $\Omega$ , we need to evaluate the strain derivatives of the various band parameters which appear in  $\Omega$ . To this end, we next use the model of the PbTe band structure which we have presented in Sec. II and the Appendix to express the strain dependence of the effective masses and cross-sectional areas in terms of the strain dependence of the Fermi energy and the band gap. We then obtain expressions

for the strain dependence of these two characteristic energies in terms of the deformation potential parameters.

The band shifts described by the deformation potential scheme lead to variation in  $\Omega$  via three types of effects. The first is due to the relative shift of the valleys produced by a shear strain. Under a shear, some of the valleys move up in energy and some move down. This relative shift of the valleys is accompanied by intervalley charge transfer and changes in the Fermi surface cross-sectional areas. Second are effects due to the nonparabolic bands. Since the energy bands of PbTe are nonparabolic, a shift in the Fermi energy also produces a change in the band parameters. Third are effects due to the strain dependence of the energy gap. The conduction- and valence-band deformation potentials are different; therefore, the energy gap is strain dependent. A change in the gap produces a change in the curvature of the bands, hence a change in band parameters. The first effect can occur only with a shear strain, whereas the last two effects will accompany both shear and dilatation strains. We will see from what follows that the dominant effect in PbTe is due to the intervalley charge transfer. This is evidenced experimentally by the fact that both the [100] ME and MS oscillations, which are the only ones to come from pure dilatation strains and involve no intervalley charge transfer, are at least an order of magnitude smaller than the oscillations along other axes.

We account quantitatively for the strain dependence of the cyclotron and band masses by differentiating Eqs. (A9) and (A5):

$$\frac{\partial \ln \mu}{\partial \epsilon_i} = C_t(\mu) \frac{\partial \ln \mu_t}{\partial \epsilon_i} + [1 - C_t(\mu)] \frac{\partial \ln \mu_l}{\partial \epsilon_i} + C_\theta(\mu) \frac{\partial \theta}{\partial \epsilon_i}, \quad (3.8)$$

$$\frac{\partial \ln m^*}{\partial \epsilon_i} = C_t(m^*) \frac{\partial \ln m_t}{\partial \epsilon_i} + [1 - C_t(m^*)] \frac{\partial \ln m_l}{\partial \epsilon_i} + C_\theta(m^*) \frac{\partial \theta}{\partial \epsilon_i}, \quad (3.9)$$

where

$$C_t(\mu) = (\mu/\mu_t)^2 [\cos^2 \theta + (\mu_t/2\mu_l) \sin^2 \theta], \quad (3.10)$$

$$C_\theta(\mu) = (\mu/\mu_t)^2 \cos \theta \sin \theta [1 - \mu_t/\mu_l], \quad (3.11)$$

and  $C_t(m^*)$  and  $C_\theta(m^*)$  are obtained from Eqs. (3.10) and (3.11) by replacing  $\mu$ ,  $\mu_t$ , and  $\mu_l$  with  $m^*$ ,  $m_t$ , and  $m_l$ , respectively. From Eqs. (2.6) and (A9) we see that the transverse masses are functions of both the Fermi energy and the energy gap. There is a further energy-gap dependence of the band-edge masses  $m_1$  and  $m_3$ , which we

discussed in Sec. II. Assuming that the effective gap is proportional to the direct gap,  $E_g \propto \Delta$ , simple differentiation gives the relations

$$\frac{\partial \ln \mu_t}{\partial \epsilon_i} = C_F \frac{\partial \ln E_F}{\partial \epsilon_i} + C_g \frac{\partial \ln E_g}{\partial \epsilon_i}, \quad (3.12)$$

$$\frac{\partial \ln \mu_l}{\partial \epsilon_i} = \frac{\partial \ln E_g}{\partial \epsilon_i}, \quad (3.13)$$

where

$$C_F = \frac{2E_F/E_g}{1 + 2E_F/E_g}, \quad (3.14)$$

$$C_g = \frac{1 + E_F/E_g}{1 + 2E_F/E_g}, \quad (3.15)$$

and, further

$$\frac{\partial \ln m_t}{\partial \epsilon_i} = C_m \frac{\partial \ln E_F}{\partial \epsilon_i} + (1 - C_m) \frac{\partial \ln E_g}{\partial \epsilon_i}, \quad (3.16)$$

$$\frac{\partial \ln m_l}{\partial \epsilon_i} = \frac{\partial \ln E_g}{\partial \epsilon_i}, \quad (3.17)$$

where

$$C_m = \frac{E_F/E_g}{1 + E_F/E_g}. \quad (3.18)$$

Equations (3.8)–(3.18) express the strain dependence of  $\mu$  and  $m^*$  in terms of the strain dependence of the energy gap, the Fermi energy, and the angle between the spheroid axis and the magnetic field.

From Eq. (A6) we see that the strain dependence of the extremal cross-sectional area is

$$\frac{\partial \ln S_m}{\partial \epsilon_i} = \frac{\partial \ln m^*}{\partial \epsilon_i} + \frac{\partial \ln E_F}{\partial \epsilon_i}. \quad (3.19)$$

Thus, using Eqs. (3.9), (3.16), and (3.17) with (3.19), we are also able to express  $\partial \ln S_m / \partial \epsilon_i$  in terms of the strain dependence of  $E_g$ ,  $E_F$ , and  $\theta$ .

We have assumed  $E_g \propto \Delta$ ; therefore,  $\partial \ln E_g / \partial \epsilon_i = \partial \ln \Delta / \partial \epsilon_i$ , which is given by Eq. (2.12). The strain dependence of the Fermi energy is computed using the constraint that the total number of carriers in the sample  $\mathcal{O}$  is independent of the strain. For our spheroidal model [see Eq. (A1)], the density of carriers in the  $\nu$ th valley is

$$p_\nu = (2^{3/2}/3\pi^2 \hbar^3) m_t m_l^{1/2} (E_F^\nu)^{3/2}. \quad (3.20)$$

Since  $\mathcal{O} = V \sum_{\nu=1}^4 p_\nu$ , where  $V$  is the crystal volume, the constraint  $\partial \mathcal{O} / \partial \epsilon_i = 0$  leads directly to

$$\delta_{1i} + \delta_{2i} + \delta_{3i} + \frac{1}{4} \left( \frac{3}{2} - C_m \right) \sum_{\nu=1}^4 \frac{\partial \ln E_g^\nu}{\partial \epsilon_i} + \left( \frac{3}{2} + C_m \right) \sum_{\nu=1}^4 \frac{\partial \ln E_F^\nu}{\partial \epsilon_i} = 0, \quad (3.21)$$

where  $\delta_{ij}$  is the Kronecker symbol, and we have used (3.16)–(3.18) to express the strain derivatives of  $m_t$  and  $m_l$  in terms of the strain derivatives of  $E_g^\nu$  and  $E_F^\nu$ . The Fermi energy for our  $p$ -type sam-

ples is the difference between the chemical potential  $\zeta$  and the valence-band maximum  $E_V^v$ ; therefore,

$$\frac{\partial \ln E_F^v}{\partial \epsilon_i} = \frac{1}{E_F} \left( \frac{\partial E_V^v}{\partial \epsilon_i} - \frac{\partial \zeta}{\partial \epsilon_i} \right). \quad (3.22)$$

Using the valence-band shifts and the gap dependence described by the deformation potential scheme, Eqs. (2.11), (2.12), (3.22), and (3.21) lead to expressions for  $\partial \ln E_F^v / \partial \epsilon_i$  in terms of the deformation potentials. There are two cases to be considered:

(i) *Dilatation strain* ( $i=1, 2$ , or  $3$ ). Equations (2.11) and (2.12) indicate that for this case all the gap and band-edge shifts are independent of  $\nu$ . Therefore, the sums in Eq. (3.21) are replaced by a multiplication factor of 4, giving

$$\frac{\partial \ln E_F^v}{\partial \epsilon_i} = - \frac{\frac{2}{3} + (1 - \frac{2}{3} C_m) G_1 / \Delta}{1 + \frac{2}{3} C_m}. \quad (3.23)$$

(ii) *Shear Strain* ( $i=4, 5$ , or  $6$ ). From Eqs. (2.11) and (2.12)

$$\sum_{\nu=1}^4 \frac{\partial \ln E_V^v}{\partial \epsilon_i} = 0 \quad \text{and} \quad \sum_{\nu=1}^4 \frac{\partial \ln E_F^v}{\partial \epsilon_i} = 0.$$

From these and Eqs. (3.21) and (3.22), it follows that  $\partial \zeta / \partial \epsilon_i = 0$ , so that

$$\frac{\partial \ln E_F^v}{\partial \epsilon_i} = \frac{1}{E_F^v} \frac{\partial E_V^v}{\partial \epsilon_i} = \pm \frac{1}{3} \frac{\bar{\epsilon}_y^v}{3E_F^v}. \quad (3.24)$$

We next examine the strain derivatives of  $\Omega$  which appear in the expression for the MS and ME oscillations, Eqs. (3.5) and (3.7), using the expressions for the strain derivatives of the band parameters Eqs. (3.8)–(3.24). Equations (3.2) and (3.3) indicate that  $\partial \Omega / \partial \epsilon_i$  contains many strain derivatives since the effective mass,  $g$  factor, Dingle temperature, cross-sectional area, and volume are, in principle, all strain dependent. However, by completely differentiating Eqs. (3.2) and (3.3) and numerically evaluating the various terms using the parameters appropriate to our PbTe samples, we find that the contribution from the strain derivative of  $S_m^v$  in the argument of the cosine factor is at least an order of magnitude larger than any other contribution. (In this numerical analysis we assume that  $\partial \ln T_D / \partial \epsilon_i$  and  $\partial \ln g / \partial \epsilon_i$  are at most as large as  $\partial \ln \mu / \partial \epsilon_i$ . Also, since the crystal strains never exceeded  $10^{-6}$  in our experiments and the cubic symmetry was only slightly perturbed, we can assume  $\partial \theta / \partial \epsilon_i \lesssim 1$ . This is equivalent to assuming that the Fermi-surface ellipsoids continue to point very nearly along the body diagonals of the strained cubic lattice.) Schematically,

$$\frac{\partial \Omega}{\partial \epsilon_i} = \frac{\partial A}{\partial \epsilon_i} \cos \left( \frac{cS_m}{e\hbar B} - \phi \right)$$

$$- A \frac{cS_m}{e\hbar B} \frac{\partial \ln S_m}{\partial \epsilon_i} \sin \left( \frac{cS_m}{e\hbar B} - \phi \right).$$

Since we find that  $\partial \ln A / \partial \epsilon_i$  is roughly of the same order as (or less than)  $\partial \ln S_m / \partial \epsilon_i$ , one of the principal factors which determines the relative magnitude of the various terms is  $cS_m / e\hbar B$ . This number is equal to  $2\pi$  times the number of Landau levels below the Fermi surface. Since our amplitude measurements were always made with oscillations corresponding to Landau numbers greater than 5, the  $\partial \ln S_m / \partial \epsilon_i$  term dominates. The fact that this is the dominant term is also borne out experimentally by the observed phase of the MS oscillations. The amplitude analysis in this work is made with that part of the data which shows only a single oscillation. This oscillation corresponds to the smallest extremal area, which we label  $S_m^0$ . Since numerical evaluation shows that the contributions to  $\partial \Omega / \partial \epsilon_i$  from other extremal areas and from harmonics ( $\lambda > 1$ ) are negligible, the expression that we use for our MS amplitude analysis takes the form

$$\frac{\partial \Omega}{\partial \epsilon_i} = -A_{10} \frac{cS_m^0}{e\hbar B} \sum_m^0 \frac{\partial \ln S_m^0}{\partial \epsilon_i} \sin \left( \frac{cS_m^0}{e\hbar B} - \phi_1 \right), \quad (3.25)$$

where the sum is over all the equivalent pieces of the Fermi surface which contribute to the given period.

We further find from numerical evaluation of the various terms in the second strain derivative of  $\Omega$  that under the experimental conditions just discussed we can write

$$\begin{aligned} \frac{\partial^2 \Omega}{\partial \epsilon_i \partial \epsilon_j} = & -A_{10} \left( \frac{cS_m^0}{e\hbar B} \right)^2 \\ & \times \sum_{s_m^0} \frac{\partial \ln S_m^0}{\partial \epsilon_i} \frac{\partial \ln S_m^0}{\partial \epsilon_j} \cos \left( \frac{cS_m^0}{e\hbar B} - \phi_1 \right). \end{aligned} \quad (3.26)$$

Equation (3.26) could include terms in  $\partial^2 S_m^0 / \partial \epsilon_i \partial \epsilon_j$ ; however, a comparison of phases in the MS and ME oscillations shows that these terms are negligible.

### C. Analytic Expressions and Ratio

Equations (3.5) and (3.25), and (3.7) and (3.26) combine to give the expressions which we use in analyzing our MS and ME experimental data,

$$\begin{aligned} \epsilon_{imn} = & A_{10} \frac{cS_m^0}{e\hbar B} \sum_{s_m^0} \sum_{i,j=1}^8 \frac{\partial \epsilon_{imn}}{\partial \epsilon_i} s_{ij}^0 \frac{\partial \ln S_m^0}{\partial \epsilon_j} \\ & \times \sin \left( \frac{cS_m^0}{e\hbar B} - \phi_1 \right), \end{aligned} \quad (3.27)$$

$$\begin{aligned} \Delta(Y_{imn})^{-1} = & A_{10} \left( \frac{cS_m^0}{e\hbar B} \right)^2 \sum_{s_m^0} \left( \sum_{i,j=1}^8 \frac{\partial \epsilon_{imn}}{\partial \epsilon_i} s_{ij}^0 \frac{\partial \ln S_m^0}{\partial \epsilon_j} \right)^2 \\ & \times \cos \left( \frac{cS_m^0}{e\hbar B} - \phi_1 \right). \end{aligned} \quad (3.28)$$

In our analysis of the experimental data we fit the MS data to Eq. (3.27) and separately fit the ME data to (3.28). We determine experimentally the values of  $A_{10}$  and  $S_m^0$  and find experimental values for the strain derivative sums which we then relate to the deformation potentials. From Eqs. (3.27) and (3.28) we see that the complicated coefficient  $A_{10}$  should disappear from the expression for the ratio of the MS and ME amplitudes for a given sample under the same thermodynamic conditions, i.e., the same  $B, T$ , crystallographic orientation, etc. It turns out, however, that we find the MS and ME Dingle temperatures  $T_D^S$  and  $T_D^Y$  to be different, leading to a term  $\exp[\alpha\mu(T_D^S - T_D^Y)/B]$  in the expression for the ratio. Even then, consideration of the ratio leads to a considerable simplification of the analysis, and we use the ratio in a separate approach to analyze the deformation potential.

#### IV. EXPERIMENTAL METHODS

The oscillatory magnetostriction was measured by determining the change in capacitance of a parallel-plate capacitor composed of one fixed plate and one plate glued directly to the end of the oriented single-crystal PbTe sample. We used a three-terminal capacitance cell based on a differential thermal expansion cell described by White,<sup>60</sup> modified to allow a variety of samples with different dimensions to be used in one cell. A ratio transformer bridge (General Radio 1615-A) and a phase-sensitive null detector were used to measure the change in capacitance. This technique allowed us to detect a change in capacitance of the order of  $10^{-6}$  pF, which corresponded to strains of a few times  $10^{-10}$ .

The magnetoelastic oscillations were measured using the mechanical composite-oscillator technique developed by Quimby and his associates.<sup>61, 62</sup> The composite oscillator consisted of a quartz bar (typical dimensions  $1 \times 0.25 \times 0.25$  cm) bonded to an oriented single-crystal PbTe bar of identical transverse dimensions. The long axis of the quartz transducer was in the  $Y$  quartz direction. The  $X$  faces of the quartz were coated with chromium-gold electrode films so that a Young's-modulus vibrational mode for the composite system was excited when a sinusoidal voltage was applied to the electrodes. The electrical leads, which also served to support the oscillator, were attached to the transducer at nodal points. The composite oscillator was driven by a frequency-stable constant-voltage source, usually at a frequency near the fundamental resonance of the transducer (typically 250 kHz). Changes in the Young's modulus of the sample as a result of an applied magnetic field produced changes in the resonance frequency of the composite oscillator (appropriate analytic ex-

pressions are given by Balamuth<sup>63</sup>) which in turn produced changes in the electrical impedance of the oscillator circuit. This impedance change was detected directly by monitoring the voltage across a small series resistor. The voltage was amplified, rectified, and applied to an  $X$ - $Y$  recorder. The response of the composite oscillator was investigated as a function of magnetic field at several driving frequencies on each side of the resonance as well as at the resonance peak itself in order to compare the changes in dispersion and attenuation of the system. In the 250-kHz range, attenuation effects were found to be completely negligible compared with the resonance-frequency shifts due to changes in the PbTe Young's modulus. Because of the high  $Q$  of the composite oscillator (typically  $10^3$ - $10^4$ ), the sensitivity was high; the minimum detectable fractional change in Young's modulus was estimated to be  $10^{-6}$ - $10^{-7}$ . It is noteworthy that even in its relatively unsophisticated form this system compares favorably in sensitivity with the sing-around ultrasonic technique commonly used to measure sound-velocity changes.<sup>63</sup>

Details of the MS and ME experimental techniques and apparatus have been described elsewhere by one of us (T. E. T.).<sup>64</sup>

#### V. EXPERIMENTAL RESULTS AND DISCUSSION

##### A. Band Parameters

Our experiments were performed on single-crystal samples from two different boules of  $p$ -type material grown by one of us (T. E. T.) by the Czochralski method. The boules were labeled X5 and X6. Samples were spark cut from neighboring sections of the middle of the boules. Hall measurements gave carrier concentrations of  $p = (3.5 \pm 0.2) \times 10^{18} \text{ cm}^{-3}$  for the X5 samples and  $p = (0.9 \pm 0.1) \times 10^{18} \text{ cm}^{-3}$  for the X6 samples. X5 [110] was a  $0.851 \times 0.488 \times 0.462$ -cm bar with long axis parallel to [110]. X5 [100]-stack was a  $0.927 \times 0.353 \times 0.36$ -cm [100]-oriented bar produced by gluing two nearly cubical pieces together with GE 7031 varnish. No magnetoelastic oscillation experiments were made with the samples from X5. The three X6 bars with axes along [100], [110], and [111] had dimensions  $0.749 \times 0.274 \times 0.312$  cm,  $0.745 \times 0.282 \times 0.244$  cm, and  $0.805 \times 0.269 \times 0.257$  cm, respectively.

The oscillation periods and phases were analyzed in terms of the factors  $\cos[2\pi/PB - \phi_1]$  in Eqs. (3.27) and (3.28). The period and phase were found by assigning successive integers  $N$  to the oscillation peaks and plotting the inverse magnetic field for the  $N$ th peak,  $B_N^{-1}$ , against  $N$ . The major oscillation periods found in this manner from the complete set of experiments are presented in

TABLE III. Measured oscillation periods and cyclotron masses.

Field direction	Period ( $10^{-6}$ G $^{-1}$ )		Cyclotron mass (units of $m_0$ )	
	X5	X6	X5	X6
[100]	...	$10.9 \pm 0.2$	...	...
[110]	$5.46 \pm 0.03$	$14.6 \pm 0.2$	$0.047 \pm 0.003$	$0.033 \pm 0.003$
[111]	$6.55 \pm 0.07$	$18.0 \pm 0.3$	$0.038 \pm 0.001$	$0.027 \pm 0.002$

Table III. The errors quoted are a combination of the standard deviation of the mean found from a least-squares fit of the data and the 0.5% field-calibration uncertainty of the magnets. These periods are in agreement with those found by Cuff *et al.*<sup>39</sup>

An important consideration in the analysis was the relative phases of the MS and ME oscillations. As Eqs. (3.27) and (3.28) show, the ME and MS oscillations for a particular sample and field orientation should be  $90^\circ$  out of phase if our model is correct. Data like those shown in Fig. 3 confirm this phase relation. The sign of the oscillation depends on the sign of

$$\sum_{i,j=1}^6 \frac{\partial \epsilon_{imn}}{\partial \epsilon_i} S_{ij}^0 \frac{\partial \ln S_m^0}{\partial \epsilon_j}$$

and the sign of  $A_{10}$ . We find that all of our data fit consistently into our analytical picture if we assume  $\gamma = \frac{1}{2}$ . This value of  $\gamma$  leads to a negative value for  $A_{10}$ , which from Eq. (3.3) corresponds to a negative value for  $\cos \frac{1}{2} \pi g \mu$ . This sign for  $\cos \frac{1}{2} \pi g \mu$  is in agreement with the  $g \mu$  values presented in Table I. A least-squares fit of all the phases within this scheme gives  $\gamma = 0.49 \pm 0.01$ .

For the spheroidal model described by Eqs. (2.2), (2.4), and (2.6) the carrier density  $p$  needed to fill four spheroids is related to the oscillation period  $P$  and the mass anisotropy  $K \equiv m_1/m_t$  by

$$p = p_0 P^{-3/2} (K \cos^2 \theta + \sin^2 \theta)^{3/4} K^{-1/4}, \quad (5.1)$$

where  $\theta$  is the angle between the major axis of the spheroid, i. e., [111], and the applied magnetic field, and  $p_0 = 2.263 \times 10^{10}$  G $^{-3/2}$  cm $^{-3}$  (a product of universal constants). Using Eq. (5.1), the periods presented in Table III, and the measured carrier concentrations, we find  $K = 6.5 (+1.0, -0.6)$  for X5 and  $K = 8.3 \pm 0.9$  for X6. In Fig. 4 we have plotted our values for  $K$  along with values found in  $p$ -type PbTe by other workers. The two most recent studies, those by Burke, Houston, and Savage<sup>47</sup> and by Schilz<sup>44</sup> indicate  $K$  values which are twice as large as those found in our work and that of three other investigators.<sup>38, 66, 67</sup> Burke *et al.* made an extensive study of Shubnikov-de Haas frequencies. They Fourier-analyzed the frequency spectrum from the three fundamental oscillations

and as many as five harmonics for numerous magnetic field directions in the (110) plane. It is quite difficult to understand the discrepancy between their results and the results of the other workers. It is noteworthy that Burke *et al.* find that the carrier concentration determined from a high-field Hall measurement agrees with that determined from the best fit of their data to Eq. (5.1). In both the work of Stiles *et al.*<sup>66</sup> and Cuff *et al.*,<sup>38</sup> the carrier concentration found from Eq. (5.1) was about 30% less than that determined from a Hall measurement for  $p \approx 3 \times 10^{18}$  cm $^{-3}$ . The latter authors attribute these extra carriers to other pieces of the Fermi surface. Analysis of Coste's data<sup>67</sup> gives reasonable agreement between the  $p$  from (5.1) and that from a Hall measurement.<sup>68</sup> Since the value of  $K$  comes into the amplitude analysis through the term  $|\partial^2 S^v / \partial p_B^2|^{-1/2}$ , Eqs. (3.3) and (A4), the contradictory  $K$  values shown in Fig. 4 will be discussed further in Sec. VB. Unless otherwise stated we will use our experimental values for  $K$ .

Cyclotron effective masses were found by measuring the ratio of the MS oscillation amplitudes at two temperatures. From Eqs. (3.27) and (3.3) the ratio of the amplitudes at the same magnetic field but at two different temperatures is given by

$$\frac{\epsilon(T_1, B)}{\epsilon(T_2, B)} = \frac{T_1 \sinh(\alpha \mu T_2 / B)}{T_2 \sinh(\alpha \mu T_1 / B)}. \quad (5.2)$$

This equation was solved by Newton's method on a digital computer for a series of oscillation peaks and temperatures. Data were normally taken near 4.2, 6.5, and 8.5 K. From a weighted least-squares fitting of the data, we find the masses presented in Table III. Since the MS amplitudes for  $\vec{B} \parallel [100]$  were very small, no masses could be determined for this field direction. No temperature-dependence studies were made for the magnetoelastic oscillations.

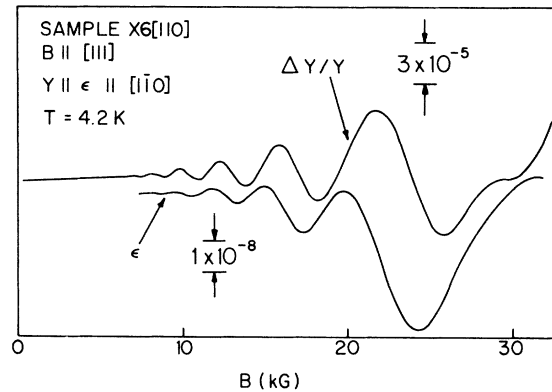


FIG. 3. Typical magnetostriction and magnetoelastic oscillation data.

From Eqs. (2.2) and (2.8) we see that  $m_t = \frac{1}{2} \times (m_1 + \mu_t m_0)$  and  $m_t = Km_t$ . Thus, from the values just presented we find  $m_t/m_0 = 0.028 \pm 0.002$ ,  $0.023 \pm 0.002$ , and  $m_t/m_0 = 0.18 \pm 0.02$ ,  $0.19 \pm 0.02$  for the X5 and X6 samples, respectively.

As a test of the internal consistency of the model, we computed the [110] cyclotron mass using Eq. (A9),  $m_t$ , the measured [111] cyclotron mass, and the measured  $K$ . The computed values are  $0.044 \pm 0.002$  and  $0.032 \pm 0.002$  for X5 and X6, respectively. The agreement between these values and the measured values shown in Table III supports the self-consistency of the model and measurements.

The Fermi energy is easily computed from the de Haas-van Alphen period and the effective mass (see the Appendix):

$$E_F = (e\hbar/m_0c)(Pm^*/m_0)^{-1}. \quad (5.3)$$

From our data for  $\vec{B} \parallel [111]$ , where  $m^* = m_t$ , we find  $E_F = 63 \pm 5$  meV and  $28 \pm 2$  meV for samples X5 and X6, respectively.

At high magnetic fields the ME and MS oscillations showed a splitting of the oscillation peaks due to the Zeeman splitting of the Landau levels. For both  $\vec{B} \parallel [111]$  and  $\vec{B} \parallel [110]$ , the oscillations from the second set of ellipsoids make the analysis ambiguous. However, from the oscillations for  $\vec{B} \parallel [100]$ , where all four ellipsoids have the same fundamental frequency, we were able to determine the spin splitting of the peaks. Each peak corre-

TABLE IV. Dingle temperatures from MS oscillations (K).

Sample and direction	Field direction			
	[110]	[ $\bar{1}\bar{1}0$ ]	[111]	[ $\bar{1}\bar{1}\bar{1}$ ]
X5[110]	$5.4 \pm 0.5$	$5.2 \pm 0.5$		$4.5 \pm 0.3$
X6[110]	$9.2 \pm 0.4$	$8.3 \pm 0.5$		$7.2 \pm 0.3$
X6[111]		$7.3 \pm 0.5$	$8.3 \pm 0.6$	

sponds to a solution of the equation

$$1/PB = N \pm \frac{1}{4} g\mu + \gamma + \frac{1}{8}, \quad (5.4)$$

where the second term on the right-hand side accounts for the two spin levels for each Landau quantum number  $N$ . This term was found by indexing the oscillation peaks with a spin index and a quantum number and plotting  $N$  vs  $(B_N^{-1})_+$  and  $(B_N^{-1})_-$ . The resulting  $g$  factors are compared in Table I with those found in  $p$ -type material by other workers. Butler and Calawa<sup>46</sup> obtained their results from magnetoemission studies in diode lasers, Schilz<sup>44</sup> from magnetoacoustic attenuation oscillations, and Cuff *et al.*<sup>39</sup> and Burke *et al.*<sup>47</sup> from Shubnikov-de Haas oscillations.

The value of  $g\mu$  depends upon the assignment of spin and quantum numbers to a set of oscillations. From the phase analysis mentioned above, we know that  $\cos \frac{1}{2} \pi g\mu$  must be negative, but this condition does not determine a unique labeling of

TABLE V. Experimental and theoretical values of the absolute value of expression (5.5) (units:  $10^{-11}$  cm<sup>2</sup> dyn<sup>-1</sup>) from MS oscillations for sample X6 ( $p = 9 \times 10^{17}$  cm<sup>-3</sup>) and X5 ( $p = 3.5 \times 10^{18}$  cm<sup>-3</sup>). The theoretical values were computed using  $\Xi_v^v = 10.46$  eV.

Sample and strain direction	X5[100]-stack				X5[110]			$\epsilon \parallel [111]$ (no sample)	
	[100]	[010]	[011]	[110]	[ $\bar{1}\bar{1}0$ ]	[001]	[ $\bar{1}\bar{1}\bar{1}$ ]	[111]	[ $\bar{1}\bar{1}0$ ]
X5 expt values	< 0.97	< 0.42	< 0.34	$6.5 \pm 0.5$	$6.3 \pm 0.7$	< 0.85	$3.5 \pm 0.4$	...	...
X5 simple theory	$0.04 \pm 0.02$	$0.04 \pm 0.02$	$0.02 \pm 0.01$	$6.9 \pm 3.6$	$7.0 \pm 3.7$	$0.04 \pm 0.02$	$3.5 \pm 1.8$	$6.9 \pm 3.6$	$4.6 \pm 2.4$
X5 full theory	$0.19 \pm 0.10$	$0.19 \pm 0.10$	$0.13 \pm 0.07$	$9.2 \pm 4.9$	$9.5 \pm 5.0$	$0.19 \pm 0.10$	$4.8 \pm 2.5$	$9.4 \pm 4.9$	$6.4 \pm 3.4$
Sample and strain direction	X6[100]			X6[110]			X6[111]		
	[100]	[010]	[011]	[110]	[ $\bar{1}\bar{1}0$ ]	[001]	[ $\bar{1}\bar{1}\bar{1}$ ]	[111]	[ $\bar{1}\bar{1}0$ ]
X6 expt values	< 4.7	...	...	$50 \pm 4$	$56 \pm 9$	< 5.7	$22 \pm 1$	$38 \pm 3$	$22 \pm 3$
X6 simple theory	$0.08 \pm 0.02$	$0.08 \pm 0.02$	$0.04 \pm 0.01$	$32.9 \pm 6.6$	$32.9 \pm 6.6$	$0.08 \pm 0.02$	$16.5 \pm 3.3$	$32.9 \pm 6.6$	$22.0 \pm 4.4$
X6 full theory	$0.30 \pm 0.06$	$0.30 \pm 0.06$	$0.18 \pm 0.04$	$38.9 \pm 7.8$	$39.3 \pm 7.9$	$0.30 \pm 0.06$	$19.8 \pm 4.0$	$39.2 \pm 7.8$	$26.2 \pm 5.2$

the oscillation peaks. The values for  $\frac{1}{2}g\mu$  in Table I correspond to a spin splitting greater than half the Landau splitting. This scheme gives  $g$  values which agree with the values found by Patel and Slusher<sup>69</sup> from spin-flip Raman scattering in *n*-type material<sup>70</sup> with  $n = 10^{17} \text{ cm}^{-3}$ .

### B. Amplitudes

The MS amplitude coefficients were found by fitting the strain oscillation amplitudes to Eqs. (3.37) and (3.3). From the data we computed the quantities  $y = \ln[\epsilon_{lmn} B^{-1/2} \sinh(\alpha\mu T/B)]$  for each oscillation peak, and a linear least-squares fit was made to a plot of  $y$  against  $B^{-1}$ . From the equations it follows that the slope of this plot gives the Dingle temperature and the  $y$  intercept leads to a value for

$$\cos \frac{1}{2}\pi g\mu \sum_{s_m^0} \sum_{i,j=1}^6 \left( \frac{\partial \epsilon_{lmn}}{\partial \epsilon_i} s_{ij}^0 \frac{\partial \ln S_m^0}{\partial \epsilon_j} \right). \quad (5.5)$$

This procedure necessitates a knowledge of  $S_m^0$ ,  $\mu$ , and  $|\partial^2 S^\nu / \partial p_\beta^2|_{S=S_m^0}^{-1/2}$  for which we use the band parameters presented in Sec. V A and Eq. (A3) of the Appendix. The Dingle temperatures found from the MS oscillations are presented in Table IV. The errors indicated are the standard deviation of the mean computed from the random error associated with the amplitude measurements and the uncertainty in  $\mu$ . The magnetostriction amplitudes for X5[100] and X6[100] were too small to give reliable Dingle temperatures.

In Table V the strain-derivative sums determined from the experimental MS amplitudes are presented

and compared with values computed from the theory of Sec. III B. The theoretical values were computed using the deformation potentials from Ferreira's theoretical work (Table II) and the elastic constants measured by Houston, Strakna, and Belson.<sup>71</sup> The extrapolated  $T=0$  K values for the stiffness constants were used to compute the following compliance constants:  $s_{11}^0 + 2s_{12}^0 = (0.731 \pm 0.007) \times 10^{-12} \text{ cm}^2 \text{ dyn}^{-1}$  and  $s_{44}^0 = (6.61 \pm 0.04) \times 10^{-12} \text{ cm}^2 \text{ dyn}^{-1}$ . The large uncertainties of the theoretical values result entirely from the uncertainty in  $\cos \frac{1}{2}\pi g\mu$ . Even though  $g\mu$  is experimentally determined to better than 10%,  $\cos \frac{1}{2}\pi g\mu$  has a large uncertainty when the function nears zero. The values in Table I lead to  $\cos \frac{1}{2}\pi g\mu = -(0.19 \pm 0.10)$  for X5 and  $-(0.40 \pm 0.08)$  for X6. The errors in the experimental strain-derivative sums are the standard deviation of the mean due to the uncertainty of the amplitude measurements and the uncertainties in  $\mu$  and  $K$ . Because of the discrepancy between the  $K$  values found by different experimenters for  $p \approx 3 \times 10^{18} \text{ cm}^{-3}$ , there is an added degree of uncertainty about the experimental values for X5, since the amplitude analysis includes the term  $|\partial^2 S^\nu / \partial p_\beta^2|^{-1/2}$  which is  $K$  dependent. For instance, if we were to use  $K=13$ , the value of Burke *et al.*, rather than our experimental value  $K=6.5$ , all of the X5 experimental values in Table V would be reduced by 23% for  $\vec{B} \parallel [100]$ , by 27% for  $\vec{B} \parallel [110]$ , and by 29% for  $\vec{B} \parallel [111]$ . Using  $K=13$  instead of 8.3 for X6 gives 17%, 19%, and 20% reductions, respectively, for these three cases. Since both  $\cos \frac{1}{2}\pi g\mu$  and  $|\partial^2 S^\nu / \partial p_\beta^2|^{-1/2}$  cancel out of the expressions for the ratio of the ME and MS ampli-

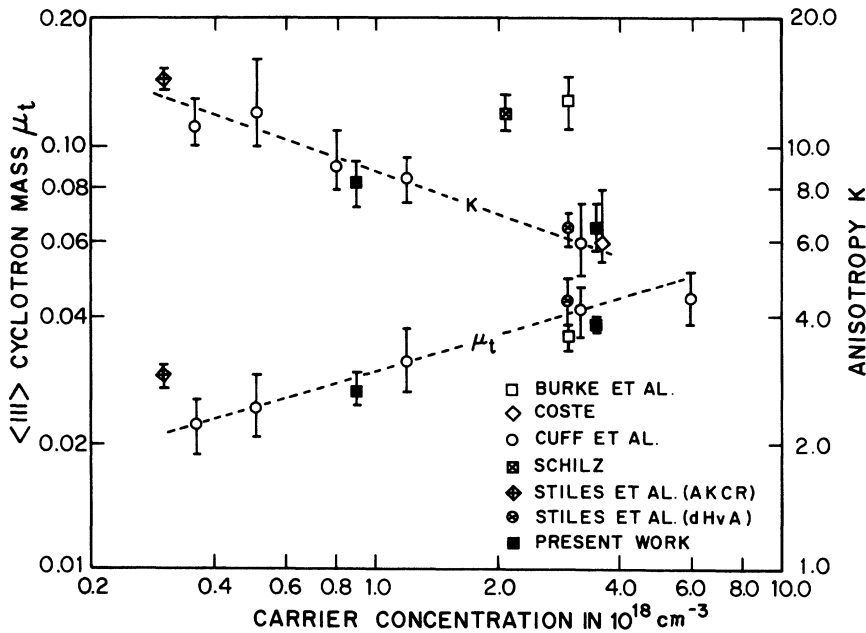


FIG. 4. Published values of the  $\langle 111 \rangle$  cyclotron mass  $\mu_t$ , and the mass anisotropy  $K$  vs carrier concentration for *p*-PbTe. See Burke *et al.*, Ref. 47; Coste, Ref. 67; Cuff *et al.*, Ref. 38; Schilz, Ref. 44; Stiles *et al.* (AKCR), Ref. 65; Stiles *et al.* (dHvA), Ref. 66.

tudes, the large uncertainties of these parameters do not enter into the results of the ratio analysis.

MS oscillations were investigated at temperatures from 4 to 9 K. No temperature dependence of the strain-derivative sums was observed, and the data in Table V are the average of values over this temperature range. The oscillations in several cases were just barely detectable or were not seen at all. For these cases an upper limit for the amplitude coefficient is presented. We had no X5[111] sample. Because the amplitudes for X6[100] were quite small for transverse magnetic field configurations, we did not attempt to align the field along specific crystallographic directions for transverse fields. These facts explain the absence of entries for the corresponding crystal and field orientations in Table V.

Two sets of theoretical values are presented in Table V. The "simple theory" values correspond to a rigid parabolic band model with infinite energy gap. In this model the strain mass term  $\partial \ln m^* / \partial \epsilon_i$  in Eq. (3.19) is neglected and  $\partial \ln S_m^0 / \partial \epsilon_i$  is considered to be due solely to the change in crystal volume ( $= -\frac{2}{3}$ ) for dilatation strains ( $i = 1, 2, \text{ or } 3$ ) or due to intervalley charge transfer ( $= \frac{1}{3} \Xi_u^v / E_F^v$ ) for shear strains ( $i = 4, 5, \text{ or } 6$ ). The values labeled "full theory" were computed using the model of Sec. III, Eqs. (3.19), (3.8), (3.16), (3.17), (3.23), (3.24), and (2.12). As an example of the magnitudes of some of the numbers which enter the theoretical computations,  $\partial \ln m^* / \partial \epsilon_i$ ,  $\partial \ln E_F / \partial \epsilon_i$ , and  $\partial \ln S_m^0 / \partial \epsilon_i$  for X6 with  $\vec{B} \parallel [110]$  are presented in Table VI.

We consider the agreement between the experimental and theoretical values in Table V to be quite reasonable; however, due to the large uncertainty in the theoretical values, especially for the X5 data, a definitive quantitative analysis of the experimental and theoretical amplitude factors is not possible with the numbers presented in Table V. However, the relative magnitudes and ratios of the various terms confirm many of the aspects of the model we have presented in Sec. III. We can see this by writing the strain derivatives in a more transparent form. When evaluating the strain-

derivative sums for the strain and field directions shown in Table V via the prescription described in Sec. IIIB, one finds that, *except* for the case  $[l, m, n] = [110]$  with  $\vec{B} \parallel [001]$ , all the sums can be simplified into the sum of a dilatation term and a shear term of the form<sup>72</sup>

$$\sum_{S_m^0} \sum_{i,j=1}^6 \frac{\partial \epsilon_{imn}}{\partial \epsilon_i} s_{ij}^0 \frac{\partial \ln S_m^0}{\partial \epsilon_j} = N_e (\beta_d + D\beta_s), \quad (5.6)$$

where  $N_e$  is the number of equivalent extremal areas  $S_m^0$ ,  $\beta_d = (s_{11}^0 + 2s_{12}^0) \partial \ln S_m^0 / \partial \epsilon_1$ ,  $\beta_s = s_{44}^0 \partial \ln S_m^0 / \partial \epsilon_4$ , and  $D$  is a direction-cosine factor which takes the values  $0, \frac{1}{2}, -\frac{1}{2}, 1$ , and  $-\frac{1}{3}$  for the  $[l, m, n]$  directions  $\langle 100 \rangle$ ,  $[110]$ ,  $[1\bar{1}0]$ ,  $[111]$ , and  $[1\bar{1}1]$ , respectively, when the derivative indicated in  $\beta_s$  is performed on the extremal area of the  $[111]$  spheroid. For the case  $[l, m, n] = [110]$  with  $\vec{B} \parallel [001]$ , the right-hand side of Eq. (5.6) becomes simply  $4\beta_d$ . A significant aspect of the model is that in this latter case the shear terms cancel when summed over the four spheroids—the shear strain causes two of the valence-band maxima to move up in energy, thereby increasing the extremal areas at the Fermi energy and the other two move down, decreasing their areas. Comparing Eq. (5.6) with the experimental data in Table V, we see that qualitatively the data fit our theoretical model quite well. We find, for example, that  $|\beta_s| \gg |\beta_d|$ ; the "full theory" values in Table VI lead to  $\beta_d = -2.2 \times 10^{-12} \text{ cm}^2 \text{ dyn}^{-1}$  and  $\beta_s = 977 \times 10^{-12} \text{ cm}^2 \text{ dyn}^{-1}$ , and these values are typical of the large difference between the dilatation and shear contributions to the strain-derivative sums predicted by our theoretical model, including other field directions and for sample X5. Since the shear term  $\beta_s$  is theoretically so much larger than the dilatation term  $\beta_d$ , any term in Eq. (5.6) which contains  $\beta_s$  will be much larger than terms which do not contain  $\beta_s$ .

From Table V we see that for all cases where Eq. (5.6) shows contributions from only the dilatation strains (i. e.,  $[l, m, n] = [100]$ ,  $D = 0$ , or a  $[110]$  strain with  $\vec{B} \parallel [001]$ ), the experimental values are at least an order of magnitude smaller than those for which Eq. (5.6) shows shear contributions. This result confirms one aspect of the model.

Another confirming aspect of the MS data comes from the ratios of various terms in Table V. Using Eq. (5.6) and assuming  $\beta_s \gg \beta_d$ , the strain-derivative sums for  $\vec{B} \parallel [110]$  with  $[l, m, n]$  along  $[110]$ ,  $[1\bar{1}0]$ , and  $[1\bar{1}1]$  should be in the ratio  $\frac{1}{2} : -\frac{1}{2} : -\frac{1}{3}$ . For  $\vec{B} \parallel [111]$  with  $[l, m, n]$  along  $[111]$  and  $[1\bar{1}0]$  the ratio should be  $1 : -\frac{1}{2}$ . The experimental data are in good agreement with these predictions. Perhaps the most striking experimental confirmation of the model comes from the observed phases. As we pointed out in Sec. V A, the phases are in complete

TABLE VI. Representative theoretical values for X6 with  $\vec{B} \parallel [110]$ .

	$\frac{\partial \ln m^*}{\partial \epsilon_i}$	$\frac{\partial \ln E_F}{\partial \epsilon_i}$	$\frac{\partial \ln S_m^0}{\partial \epsilon_i}$
Simple theory			
$i = 1, 2, \text{ or } 3$	0	$-\frac{2}{3}$	$-\frac{2}{3}$
$i = 4, 5, \text{ or } 6$	0	124.5	124.5
Full theory			
$i = 1, 2, \text{ or } 3$	12.6	- 15.7	- 3.1
$i = 4, 5, \text{ or } 6$	23.5	124.5	148.0

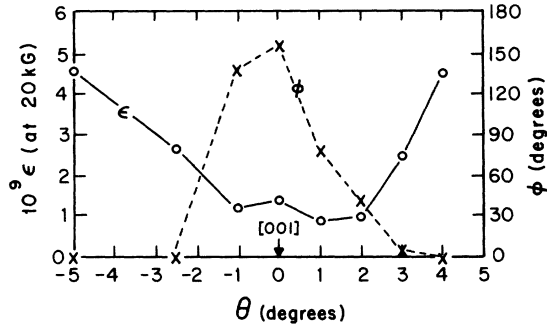


FIG. 5. Amplitude  $\epsilon$  and phase  $\phi$  of [110] magnetostriction oscillations for  $\vec{B}$  near [001] for sample X6.

agreement with our model; e.g., the MS oscillations for  $\vec{B} \parallel [110]$  with  $[l, m, n] \parallel [110]$  and  $[1\bar{1}0]$  are  $180^\circ$  out of phase, as we would expect from Eq. (5.6).

The observed changes in amplitude and the phase shifts of the MS oscillations due to cancellation of the shear terms as the magnetic field is rotated into the [001] direction in the (110) plane are shown by the experimental data in Fig. 5. The experimental results with  $\vec{B}$  or  $[l, m, n]$  along  $\langle 100 \rangle$  are difficult to analyze because the strain amplitudes are quite small and any slight misalignment of the sample would produce an anomalously large signal. This fact is made quite apparent by Fig. 5.

The ME amplitude analysis is quite similar to the MS analysis. A linear least-squares fit was made of

$$x = \ln[\Delta(Y_{l,mn})^{-1} B^{1/2} \sinh(\alpha \mu T/B)]$$

against  $B^{-1}$ . From Eqs. (3.28) and (3.3) it follows that the Dingle temperature comes from the slope of the curve and the  $x$  intercept gives a value for

$$\cos \frac{1}{2} \pi g \mu \sum_m^0 \left( \sum_{i,j=1}^6 \frac{\partial \epsilon_{lmn}}{\partial \epsilon_i} s_{ij}^0 \frac{\partial \ln S_m^0}{\partial \epsilon_j} \right)^2. \quad (5.7)$$

The Dingle temperatures found from the ME amplitude analysis are presented in Table VII. The ME Dingle temperatures for  $\vec{B} \parallel (110)$  are consistently lower than the MS Dingle temperatures for the same samples, whereas for  $\vec{B} \parallel \langle 111 \rangle$  the ME Dingle temperatures are larger than the MS Dingle

temperatures. This result is unexpected within the framework of our model.

Table VIII shows theoretical and experimental values determined for the ME strain-derivative sums. The "simple theory" and "full theory" values have the same meaning as for the MS theoretical values. The elastic constants, deformation potentials, and the value of  $\cos \frac{1}{2} \pi g \mu$  used for the theoretical evaluations are the same as those used to calculate the MS amplitude terms. Again, the uncertainty in the theoretical values comes from the uncertainty in  $\cos \frac{1}{2} \pi g \mu$ . Recall also that the experimental values depend upon the value of  $K$  used in the data reduction. Using  $K = 13$  instead of 8.3 leads to a reduction of the experimental values by 17%, 19%, and 20% for the [100], [110], and [111] magnetic field directions, respectively.

Just as we were able to write the MS strain derivative sums in a form which illuminates the significance of the relative magnitudes of the values in Table V, we find that the ME strain-derivative sums for all the sample and field directions shown in Table VII, *except* the case  $[l, m, n] = [110]$  with  $\vec{B} \parallel [001]$ , can be expressed in the form

$$\sum_m^0 \left( \sum_{i,j=1}^6 \frac{\partial \epsilon_{lmn}}{\partial \epsilon_i} s_{ij}^0 \frac{\partial \ln S_m^0}{\partial \epsilon_j} \right)^2 = N_e (\beta_d + D\beta_s)^2, \quad (5.8)$$

where all the terms have the same meaning as in Eq. (5.6). For the case  $[l, m, n] = [110]$  with  $\vec{B} \parallel [001]$ , the right-hand side of Eq. (5.8) becomes  $4(\beta_d^2 + \frac{1}{4}\beta_s^2)$ . Remember that for the comparable MS case the shear terms  $\beta_s$  cancelled out when summed over the four spheroids. In the ME case the strain derivatives are all squared before they are summed, and the shear term does not cancel. Since  $|\beta_s| \gg |\beta_d|$ , as seen experimentally and theoretically from both the MS and ME data, the MS strain-derivative sum for the case  $[l, m, n] = [110]$  with  $\vec{B} \parallel [001]$  was an order of magnitude less than the sums involving  $\beta_s$ . In contrast, the ME strain-derivative sum for this orientation is seen to be of the same magnitude as in the other cases.

Using  $|\beta_s| \gg |\beta_d|$ , Eq. (5.8) predicts that for X6[110] the ratio of the strain-derivative sums for  $\vec{B} \parallel [110]$ ,  $[1\bar{1}0]$ ,  $[001]$ , and  $[1\bar{1}1]$ , respectively, should be 2:2:4:1. The experimental values confirm this aspect of the theoretical model rea-

TABLE VII. Dingle temperatures from ME oscillations (K).

Sample and axis	Field direction					
	[100]	[001]	[110]	[1 $\bar{1}$ 0]	[111]	[1 $\bar{1}$ 1]
X6[100]	9.6 ± 0.8	8.3 ± 1.0		6.8 ± 0.9		
X6[110]		8.4 ± 0.4	8.5 ± 0.4	7.5 ± 0.3		8.2 ± 0.5
X6[111]				7.3 ± 0.5	10.2 ± 0.2	

TABLE VIII. Experimental and theoretical values of expression (5.7) in the text (units:  $10^{-20}$  cm<sup>4</sup> dyn<sup>-2</sup>) from ME oscillations for sample X6. The theoretical values were computed using  $\Xi_u^v = 10.46$  eV.

Sample and axis	X6[100]			X6[110]			X6[111]		
	[100]	[010]	[011]	[110]	[1 $\bar{1}$ 0]	[001]	[1 $\bar{1}$ 1]	[111]	[1 $\bar{1}$ 0]
Field direction									
Experimental values	3.1±0.7	2.9±0.9	1.3±0.3	23±3	15±2	33±4	9.7±1.6	2.7±0.4	2.6±0.3
Simple theory	0.0	0.0	0.0	13.5±2.7	13.5±2.7	27±5	6.8±1.4	27±5	6±1
Full theory	0.0	0.0	0.0	18.9±3.8	19.3±3.9	37±7	9.8±2.0	38.5±7.7	8.6±1.7

sonably well. The experimental values for X6[110] are also in reasonably good agreement with those predicted by the theoretical model. The fact that the ME theoretical values predicted for X6[100] are much smaller than the values measured is not too surprising since our model and calculations contain several simplifying assumptions. The X6[100] experimental values are, in fact, an order of magnitude smaller than the X6[110] experimental values. This we understand qualitatively within the framework of our model. The order-of-magnitude disagreement between experiment and theory for X6[111] is not understood at this time. The experiments on X6[111] were carefully repeated in an unsuccessful attempt to resolve this discrepancy. Equation (5.8) predicts that the strain-derivative sum for X6[111] with  $\vec{B} \parallel [111]$  should be equal to the X6[110] value for  $\vec{B} \parallel [001]$  and that the value for the X6[111] case with  $\vec{B} \parallel [1\bar{1}0]$  should be  $\frac{2}{9}$  of this value. The MS data for X6[111] gave good agreement between experiment and theory, so the discrepancy does not seem to be associated with this particular sample.

We have already pointed out in Sec. III C that the expression for the ratio of the ME to the MS amplitudes is greatly simplified owing to the cancellation of most of the coefficient  $A_{10}$  which contains, among other things, a  $K$  factor term and  $\cos \frac{1}{2} \pi g \mu$ . From Eqs. (3.27), (3.28), (5.6), and (5.8) we see that for all the sample configurations in Tables V and VII, *except* the case  $[l, m, n] = [110]$  with  $\vec{B} \parallel [001]$ , the expression for the ratio of the amplitudes takes the form

$$\frac{\Delta(Y_{lmn})^{-1}}{\epsilon_{lmn}} = \frac{cS_m^0}{e\hbar B} \sum_{s_m^0} \sum_{i,j=1}^6 \frac{\partial \epsilon_{lmn}}{\partial \epsilon_i} s_{ij}^0 \frac{\partial \ln S_m^0}{\partial \epsilon_j} e^{\alpha \mu (T_D^e - T_B^f) / B}. \quad (5.9)$$

If the Dingle temperatures were the same, the right-hand side of Eq. (5.9) would have a simple

$B^{-1}$  field dependence. The experimentally observed field dependence does, in fact, deviate from  $B^{-1}$ , and we attribute this wholly to the difference in Dingle temperatures.

Since the X6[100] amplitudes are too small and the X6[111] ME data are questionable, we have only the data from X6[110] for the ratio. (No ME measurements were made on the X5 samples.) By least-squares fitting a semilog plot of Eq. (5.9) for the data from X6[110], we find the parameters presented in Tables IX and X. As can readily be seen from Table IX, the ME and MS Dingle-temperature difference determined from the ratio, Eq. (5.9), and the difference obtained from the values from the two separate experiments agree quite well. The nature of this difference is not understood within the framework of our thermodynamic model.

The strain-derivative sums determined from the ratio are displayed in Table X. The terms "simple theory" and "full theory" have the same meanings as above. The experimental values for the ratio are independent of the  $K$  value and the  $\cos \frac{1}{2} \pi g \mu$  so that uncertainties in these parameters have no effect on the results. The uncertainties of the experimental values in Table X are mainly due to the random uncertainties of the amplitude measurements themselves.

TABLE IX. Difference between the MS and ME Dingle temperatures,  $T_D^e - T_B^f$  (K).

Sample and axis	X6[110]		
	[110]	[1 $\bar{1}$ 0]	[1 $\bar{1}$ 1]
Field direction			
From Eq. (5.9) <sup>a</sup>	1.4±0.1	1.3±0.7	-1.2±0.2
From Tables IV and VII <sup>b</sup>	0.7±0.6	0.8±0.6	-1.0±0.6

<sup>a</sup>Fitting the ME-MS ratio data to Eq. (5.9).

<sup>b</sup>Difference between the values determined by the two separate experiments.

TABLE X. Absolute value of expression (5.6) in the text (units:  $10^{-11}$  cm<sup>2</sup> dyn<sup>-1</sup>) determined from the ME-MS amplitude ratio, using  $\Xi_u^v = 7.9 \pm 1.3$  eV for the theoretical values.

Sample and axis	X6[110]		
	[110]	[ $\bar{1}\bar{1}0$ ]	[ $\bar{1}\bar{1}1$ ]
Experimental values	$37 \pm 2$	$26 \pm 5$	$48 \pm 3$
Simple theory	$31 \pm 5$	$31 \pm 5$	$31 \pm 5$
Full theory	$37 \pm 6$	$37 \pm 6$	$37 \pm 6$

From our theoretical model [see, for instance, Table VI and Eq. (3.24)] we find that the strain-derivative sums shown in Table X are essentially linearly proportional to  $\Xi_u^v$ ; therefore, for the theoretical values in Table X we have scaled the deformation potential to give the best fit of the theory to the experiment. The best value  $\Xi_u^v = 7.9 \pm 1.3$  eV is in good agreement with the value 8.5 eV found from piezoresistance measurements by Burke.<sup>56</sup> When we scale the ME data above for a best fit between experiment and theory, we find  $\Xi_u^v = 10.1 \pm 1.2$  eV. The uncertainty in the deformation potential determined from the ME data above comes mainly from the uncertainty in  $\cos \frac{1}{2} \pi g \mu$ . For the ME case, however, we must concern ourselves with the question of whether  $K$  is more like 13 or 8.3. The 10% uncertainty introduced by this difference is not included in the  $\pm 1.2$  eV.

Having found a value for the deformation potential from the MS-ME amplitude ratio, we next return to the MS and ME data to find a value for  $\cos \frac{1}{2} \pi g \mu$ . Taking  $\Xi_u^v = 7.9 \pm 1.3$  eV, we use our theoretical model to compute values for the strain-derivative sums and then combine these results with Eqs. (3.27) and (3.28) and the experimental amplitudes to find  $\cos \frac{1}{2} \pi g \mu$ . The results of this procedure are given in Table XI. The comparison of the spin factor found in this manner with the value found directly from the splitting of the oscillation peaks is a further test of the internal consistency of the theoretical model. Assuming  $\cos \frac{1}{2} \pi g \mu$  to be the same in the [100], [110], and

[111] directions, and incorporating our phase results which indicate that this function must be negative, the average of the X5 values in Table XI give  $\cos \frac{1}{2} \pi g \mu = -(0.18 \pm 0.02)$  compared with the spin-splitting value of  $-(0.19 \pm 0.10)$ . The X6 values average to  $-(0.57 \pm 0.06)$  compared with the spin-splitting value of  $-(0.40 \pm 0.08)$ . For this analysis we have used our own values for  $K$ . If we had used the  $K$  value of Burke *et al.*, the X5 and X6 data in Table XI would have to be shifted down by 28% and 15%, respectively. If our model is correct this indicates that a value of  $K = 13$  for  $p = 3 \times 10^{18}$  cm<sup>-3</sup> is too high.

## VI. SUMMARY AND CONCLUSIONS

We have presented a detailed experimental and theoretical study of quantum oscillations in the magnetostriction (oscillatory magnetostriction) and Young's modulus (magnetoelastic oscillations) of  $p$ -PbTe. The latter represents the first observation of quantum oscillations in the elastic constants of a semiconductor. In the theory, the oscillatory magnetostriction and magnetoelastic oscillations are related to strain derivatives of extremal Fermi-surface cross-sectional areas using appropriate thermodynamic derivatives of the modified Lifshitz-Kosevich expression for the quantum oscillatory electronic free energy. These strain derivatives are in turn related to a deformation potential description of the strain dependence of the electronic band structure using an adaptation of Cohen's nonellipsoidal nonparabolic band model to describe the nearly spheroidal nonparabolic valence band of PbTe.

From the periods, phases, and spin splitting of the oscillations, we find experimental band parameters for  $p$ -PbTe which are in generally good agreement with parameters reported by other workers, although there is a discrepancy with recent results of Burke, Houston, and Savage<sup>47</sup> and of Schilz<sup>44</sup> in the value of the Fermi-surface anisotropy constant  $K$ . These latter workers found values of  $K$  near 13 for carrier concentrations near  $3 \times 10^{18}$  cm<sup>-3</sup>, whereas we found  $K = 6.5$  for  $p = 3.5 \times 10^{18}$  cm<sup>-3</sup>.

The absolute amplitudes of the magnetostriction and magnetoelastic oscillations were generally in

TABLE XI.  $|\cos \frac{1}{2} \pi g \mu|$  determined from MS and ME amplitude data assuming  $\Xi_u^v = 7.9 \pm 1.3$  eV.

Effect, sample, and axis	Field direction				
	[110]	[ $\bar{1}\bar{1}0$ ]	[001]	[ $\bar{1}\bar{1}1$ ]	[111]
MS X5[110]	$0.18 \pm 0.03$	$0.17 \pm 0.03$		$0.18 \pm 0.04$	
MS X6[110]	$0.68 \pm 0.13$	$0.76 \pm 0.18$		$0.59 \pm 0.10$	
MS X6[111]		$0.44 \pm 0.10$			$0.52 \pm 0.10$
ME X6[110]	$0.86 \pm 0.33$	$0.55 \pm 0.21$	$0.63 \pm 0.24$	$0.70 \pm 0.28$	

good agreement with the predictions of our theory. From the *ratio* of the amplitudes of the two types of oscillation we have derived a value of the valence-band deformation potential  $\Xi_v^0 = 7.9 \pm 1.3$  eV. This agrees well with the value 8.5 eV previously obtained by Burke<sup>56</sup> from piezoresistance measurements. The relative phase of the two types of oscillation is in accord with that predicted by the theory. A detailed study of the absolute amplitudes of the two types of oscillations indicates that the dominant effect of strain on the valence band is a lifting of the degeneracy of the valence-band maxima by shear strains accompanied by intervalley charge transfer. The effects of strain on the band parameters (the so-called strain-mass effects) are roughly an order of magnitude smaller than the intervalley charge-transfer effects. This is in contradiction with a conclusion of Belson *et al.*<sup>16</sup> based on oscillatory magnetostriction experiments only. In their analysis these workers used band parameters from the literature which give a value of the spin-splitting factor in disagreement with our experimental observations, and in addition their analysis appears to contain a numerical error. If these two features of their analysis are corrected, their results are seen to be consistent with small strain-mass effects. Study of our amplitude results also suggests that our value of the Fermi-surface anisotropy constant is more nearly correct than the higher values reported by Burke, Houston, and Savage, and by Schilz.

#### APPENDIX

In this appendix we present some basic relationships between the band parameters for our spheroidal nonparabolic energy-band model of PbTe. Most of the relations follow directly from geometric considerations.

The four  $\langle 111 \rangle$  spheroidal bands described by Eqs. (2.2), (2.4), and (2.6) can accommodate a total carrier density  $p$  if the volume  $V_p$  in momentum space of each spheroid is

$$V_p(E_F) = (p/8) h^3 = \frac{4}{3} \pi m_t E_F (2m_t E_F)^{1/2}.$$

This requires that the Fermi energy  $E_F$  be

$$E_F = \frac{\hbar^2 (3\pi^2 p/4)^{2/3}}{2m_t K^{1/3}}. \quad (\text{A1})$$

From straightforward geometrical considerations the area of intersection  $S$  between a plane perpendicular to an axis  $p_B$  and a spheroidal Fermi surface is found to be

$$S(\theta, p_B) = \frac{2\pi m_t \sqrt{K E_F}}{(K \cos^2 \theta + \sin^2 \theta)^{1/2}} - \frac{\pi p_B^2 \sqrt{K}}{(K \cos^2 \theta + \sin^2 \theta)^{3/2}}, \quad (\text{A2})$$

where  $\theta$  is the angle between the  $p_B$  axis and the spheroid axis and  $p_B$  is the distance from the plane to the center of the spheroid.

The period of the quantum oscillations is determined by the maximum cross-sectional area  $S_m$  of the Fermi surface perpendicular to the field direction,  $P = eh/cS_m$ . From (A2) we see that the maximum cross-sectional area occurs when  $p_B = 0$ , giving

$$P(\theta) = \frac{e\hbar(K \cos^2 \theta + \sin^2 \theta)^{1/2}}{cm_t \sqrt{K E_F}}. \quad (\text{A3})$$

From (A2) we can evaluate one of the important amplitude factors of the Lifshitz-Kosevich equation [Eq. (3.3)]:

$$\left| \frac{\partial^2 S}{\partial p_B^2} \right|_{S=S_m}^{-1/2} = \left( \frac{K}{2\pi} \right)^{1/2} [\cos^2 \theta + (\sin^2 \theta)/K]^{3/4}. \quad (\text{A4})$$

It is convenient to define a band mass  $m^*$  for the nonparabolic bands by the relation

$$\left( \frac{1}{m^*} \right)^2 \equiv \frac{\cos^2 \theta}{m_t^2} + \frac{\sin^2 \theta}{m_t m_l}. \quad (\text{A5})$$

The preceding expressions can be written more easily in terms of this band mass:

$$S_m(\theta) = 2\pi m^* E_F, \quad (\text{A6})$$

$$P(\theta) = e\hbar/cE_F m^*, \quad (\text{A7})$$

$$\left| \frac{\partial^2 S}{\partial p_B^2} \right|_{S=S_m}^{-1/2} = \left( \frac{K}{2\pi} \right)^{1/2} \left( \frac{m_t}{m^*} \right)^{3/2}. \quad (\text{A8})$$

The reduced cyclotron mass for a magnetic field in the  $B$  direction is defined as  $\mu = (1/2\pi m_0)(\partial S_m / \partial E)_{E_F}$ . Substituting Eq. (2.6) into Eq. (A2) and differentiating, we find

$$\left( \frac{1}{\mu} \right)^2 = \left( \frac{\cos^2 \theta}{\mu_t^2} + \frac{\sin^2 \theta}{\mu_t \mu_l} \right) \Phi, \quad (\text{A9})$$

where  $\mu_t = (m_1/m_0)(1 + 2E_F/E_g)$ ,  $\mu_l = m_3/m_0$ , and  $\Phi = (1 - \xi)(1 + 2r)^2(1 + 2r - r\omega)^{-2}$ , where  $r \equiv E_F/E_g$ ,  $\omega = \frac{1}{2}(1 + r)[1 + r + (m_3/m_1)\cot^2 \theta]^{-1}$ , and  $\xi = r[1 + 2r + (m_3/m_1)\cot^2 \theta]^{-1}$ . Using the experimental results for PbTe from Sec. V A,  $\Phi$  is found to be very near 1 when the field is in any of the principal crystallographic directions: For the X6 samples  $0.99 < \Phi < 1$ , and for X5,  $0.97 < \Phi < 1$ . Thus, for all practical purposes we can set  $\Phi = 1$ . Notice that  $\mu_t \neq m_t/m_0$ , except for  $E_F/E_g = 0$ .

†Work supported by the Advanced Research Projects Agency and the U. S. Air Force Office of Scientific Research, Office of Aerospace Research, under Contract No. F44620-69-C-0077. Based on a thesis submitted by T. E. Thompson in partial fulfillment of the requirements for the Ph. D. degree at the University of Pennsylvania.

\*Present address: The Moore School of Electrical Engineering, University of Pennsylvania, Philadelphia, Pa. 19104.

<sup>1</sup>For an excellent review with extensive references, see A. V. Gold, in *Solid State Physics*, edited by J. F. Cochran and R. R. Haering (Gordon and Breach, New York, 1968), Vol. 1, p. 39.

<sup>2</sup>J. P. Joule, *Ann. Elec.* **8**, 219 (1842).

<sup>3</sup>P. Kapitza, *Nature* **124**, 53 (1929); *Proc. Roy. Soc. (London)* **A135**, 537 (1932).

<sup>4</sup>B. S. Chandrasekhar, *Phys. Letters* **6**, 27 (1963).

<sup>5</sup>B. A. Green and B. S. Chandrasekhar, *Phys. Rev. Letters* **11**, 331 (1963).

<sup>6</sup>P. R. Aron, *Bull. Am. Phys. Soc.* **15**, 263 (1970).

<sup>7</sup>T. E. Thompson, *Bull. Am. Phys. Soc.* **15**, 264 (1970).

<sup>8</sup>B. S. Chandrasekhar, E. Fawcett, D. M. Sparlin, and G. K. White, in *Proceedings of the Tenth International Conference on Low Temperature Physics, Moscow, 1966*, edited by M. P. Malkov (Viniti, Moscow, 1967), Vol. 3, p. 328.

<sup>9</sup>P. R. Aron and B. S. Chandrasekhar, *Phys. Letters* **30A**, 86 (1969).

<sup>10</sup>D. M. Sparlin and J. M. Carter, *Bull. Am. Phys. Soc.* **15**, 270 (1970).

<sup>11</sup>E. Fawcett, *Bull. Am. Phys. Soc.* **15**, 264 (1970).

<sup>12</sup>A. J. Slavin, M.S. dissertation (University of Toronto, 1968) (unpublished).

<sup>13</sup>P. A. Penz (private communication).

<sup>14</sup>B. S. Chandrasekhar, J. H. Condon, E. Fawcett, and W. M. Becker, *Phys. Rev. Letters* **17**, 954 (1966).

<sup>15</sup>P. R. Aron, B. S. Chandrasekhar, and T. E. Thompson (unpublished).

<sup>16</sup>H. S. Belson, J. R. Burke, E. Callen, B. Houston, H. Savage, J. Babiskin, and P. G. Siebenmann, *Phys. Rev. Letters* **19**, 1429 (1967).

<sup>17</sup>V. N. Mahajan and D. M. Sparlin, *Bull. Am. Phys. Soc.* **12**, 286 (1967).

<sup>18</sup>M. M. Finkelstein (private communication).

<sup>19</sup>L. Reitz and D. M. Sparlin, *Bull. Am. Phys. Soc.* **11**, 169 (1966).

<sup>20</sup>P. R. Aron (unpublished).

<sup>21</sup>D. Shoenberg (private communication). See Ref. 14.

<sup>22</sup>See, e.g., J. F. Nye, *Physical Properties of Crystals* (Clarendon, Oxford, England, 1957), Chap. 8, p. 134.

<sup>23</sup>See Eq. (3.2).

<sup>24</sup>J. G. Mavroides, B. Lax, K. J. Button, and Y. Shapira, *Phys. Rev. Letters* **9**, 451 (1962).

<sup>25</sup>A. G. Beattie, *Bull. Am. Phys. Soc.* **14**, 400 (1969).

<sup>26</sup>G. A. Alers and R. T. Swim, *Phys. Rev. Letters* **11**, 72 (1963).

<sup>27</sup>L. R. Testardi and J. H. Condon, *Phys. Rev. B* **1**, 3928 (1970).

<sup>28</sup>L. J. Neuringer and Y. Shapira, *Phys. Rev.* **165**, 751 (1968).

<sup>29</sup>T. E. Thompson and D. N. Langenberg, *Solid State Commun.* **8**, 1503 (1970).

<sup>30</sup>A. G. Beattie and E. A. Uehling, *Phys. Rev.* **148**, 657 (1966).

<sup>31</sup>V. L. Gurevich, V. G. Skobov, and Yu. A. Firsov, *Zh. Eksperim. i Teor. Fiz.* **40**, 786 (1961) [*Sov. Phys. JETP* **13**, 552 (1961)].

<sup>32</sup>D. N. Langenberg, J. J. Quinn, and S. Rodriguez, *Phys. Rev. Letters* **12**, 104 (1964).

<sup>33</sup>J. J. Quinn and S. Rodriguez, *Phys. Rev. Letters* **9**, 145 (1962).

<sup>34</sup>S. Rodriguez, *Phys. Rev.* **132**, 535 (1963).

<sup>35</sup>A. Ya. Blank and E. A. Kaner, *Zh. Eksperim. i Teor. Fiz.* **50**, 1013 (1966) [*Sov. Phys. JETP* **23**, 673 (1966)].

<sup>36</sup>V. I. Pustovoi and I. A. Poluéktov, *Zh. Eksperim. i Teor. Fiz.* **50**, 1265 (1966) [*Sov. Phys. JETP* **23**, 841 (1966)].

<sup>37</sup>See the references in the beginning of P. J. Lin and L. Kleinman, *Phys. Rev.* **142**, 478 (1966).

<sup>38</sup>K. F. Cuff, M. R. Ellett, and C. D. Kuglin, in *Proceedings of the International Conference on the Physics of Semiconductors, Exeter, 1962*, edited by A. C. Strickland (The Institute of Physics and The Physical Society, London, 1962), p. 316.

<sup>39</sup>K. F. Cuff, M. R. Ellett, C. D. Kuglin, and L. R. Williams, in *Proceedings of the Seventh International Conference on the Physics of Semiconductors, Paris, 1964*, edited by M. Hulin (Dunod, Paris, 1964), p. 677.

<sup>40</sup>J. R. Dixon and H. R. Riedl, *Phys. Rev.* **138**, A873 (1965).

<sup>41</sup>E. O. Kane, *J. Phys. Chem. Solids* **1**, 249 (1957).

<sup>42</sup>M. H. Cohen, *Phys. Rev.* **121**, 387 (1961).

<sup>43</sup>K. F. Cuff, M. R. Ellett, and C. D. Kuglin, *J. Appl. Phys. Suppl.* **32**, 2179 (1961).

<sup>44</sup>W. Schilz, *J. Phys. Chem. Solids* **30**, 893 (1969).

<sup>45</sup>D. L. Mitchell, E. D. Palik, and J. N. Zemel in *Ref. 39*, p. 325.

<sup>46</sup>J. F. Butler and A. R. Calawa, in *Physics of Quantum Electronics*, edited by P. L. Kelley, B. Lax, and P. E. Tannenwald (McGraw-Hill, New York, 1966), p. 458.

<sup>47</sup>J. R. Burke, B. Houston, and H. T. Savage, *Phys. Rev. B* **2**, 1977 (1970).

<sup>48</sup>L. M. Roth, *Phys. Rev.* **118**, 1534 (1960).

<sup>49</sup>M. H. Cohen and E. I. Blount, *Phil. Mag.* **5**, 115 (1960).

<sup>50</sup>There is, in fact, the spin degeneracy; however, for the rock-salt structure, this degeneracy is never destroyed by strain deformation. See Ref. 54, below.

<sup>51</sup>J. Bardeen and W. Shockley, *Phys. Rev.* **80**, 72 (1950).

<sup>52</sup>C. Herring, *Bell System Tech. J.* **34**, 237 (1955).

<sup>53</sup>C. Herring and E. Vogt, *Phys. Rev.* **101**, 944 (1956).

<sup>54</sup>L. G. Ferreira, *Phys. Rev.* **137**, A1601 (1965).

<sup>55</sup>Y. V. Ilisavskii, *Fiz. Tverd. Tela* **4**, 918 (1962) [*Sov. Phys. Solid State* **4**, 674 (1962)].

<sup>56</sup>J. R. Burke, *Phys. Rev.* **160**, 636 (1967).

<sup>57</sup>Values quoted in Ref. 54.

<sup>58</sup>See, e.g., J. H. Condon, *Phys. Rev.* **145**, 526 (1966).

<sup>59</sup>S. J. Williamson, S. Foner, and R. A. White, *Phys. Rev.* **136**, A1065 (1965).

<sup>60</sup>G. K. White, *Cryogenics* **1**, 151 (1961).

<sup>61</sup>S. L. Quimby, *Phys. Rev.* **25**, 558 (1925).

<sup>62</sup>L. Balamuth, *Phys. Rev.* **45**, 715 (1934).

<sup>63</sup>R. L. Forgas, *IRE Trans. Instr.* **1-9**, 359 (1960).

<sup>64</sup>T. E. Thompson, Ph.D. thesis (University of Pennsylvania, 1969) (unpublished).

<sup>65</sup>P. J. Stiles, E. Burstein, and D. N. Langenberg,

Phys. Rev. Letters 9, 257 (1962).

<sup>66</sup>P. J. Stiles, E. Burstein, and D. N. Langenberg, J. Appl. Phys. Suppl. 32, 2174 (1961).

<sup>67</sup>G. Coste, Phys. Status Solidi 20, 361 (1967).

<sup>68</sup>In his paper Coste claims that these two values do not agree, but his computation of  $p$  seems to be in error.

<sup>69</sup>C. K. N. Patel and R. E. Slusher, Phys. Rev. 177, 1200 (1969).

<sup>70</sup>Because of the similarities between the PbTe conduction and valence bands, the  $g$  values (as well as effective masses) should be comparable in  $n$ - and  $p$ -type material.

<sup>71</sup>B. Houston, R. E. Strakna, and H. S. Belson, J. Appl. Phys. 39, 3913 (1968).

<sup>72</sup>Straightforward, although tedious, symmetry considerations appropriate to the  $m3m$  symmetry of PbTe can also be used to find these relationships.